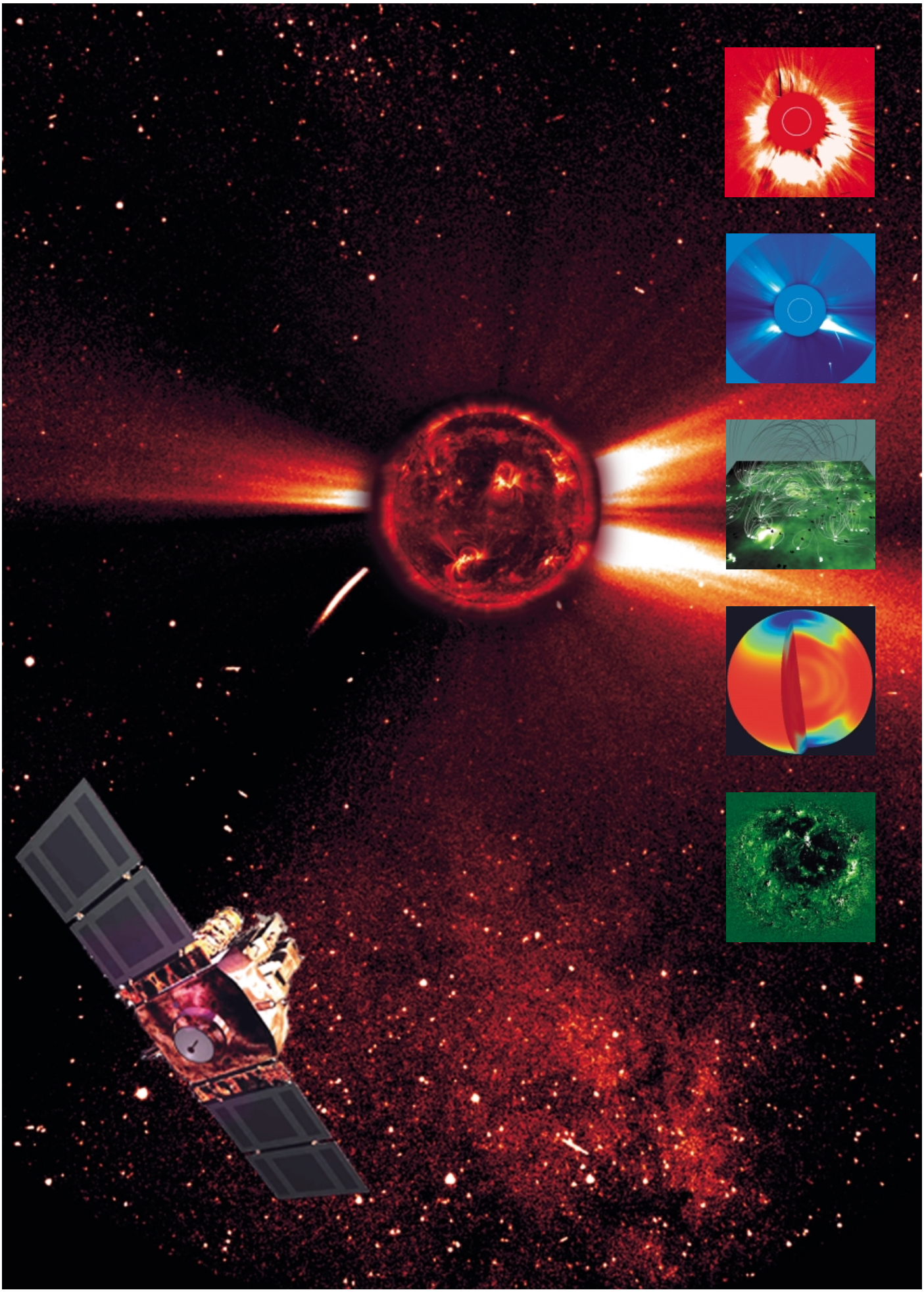

Four Years of SOHO Discoveries – Some Highlights

B. Fleck, P. Brekke, S. Haugan & L. Sanchez Duarte
Solar System Division, ESA Space Science Department, NASA/GSFC, Greenbelt, Maryland, USA

V. Domingo
Department of Astronomy and Meteorology, University of Barcelona, Spain

J.B. Gurman & A.I. Poland
Laboratory for Astronomy and Solar Physics, NASA/GSFC, Greenbelt, Maryland, USA

Since its launch on 2 December 1995, the Solar and Heliospheric Observatory (SOHO) has provided an unparalleled breadth and depth of information about the Sun, from its interior, through the hot and dynamic atmosphere, out to the solar wind. Analysis of the helioseismology data from SOHO has shed new light on a number of structural and dynamic phenomena in the solar interior, such as the absence of differential rotation in the radiative zone, subsurface zonal and meridional flows, sub-convection-zone mixing, a possible circumpolar jet, and very slow polar rotation. The ultraviolet imagers and spectrometers have revealed an extremely dynamic solar atmosphere in which plasma flows play an important role. Evidence for an upward transfer of magnetic energy from the Sun's surface toward the corona has been found. Electrons in coronal holes have been found to be relatively 'cool', whereas heavy ions are extremely hot and have highly anisotropic velocity distributions. The source region for the high-speed solar wind has been identified and the acceleration profiles of both the slow and fast solar wind have been measured.

The SOHO mission

SOHO, the Solar and Heliospheric Observatory, is an international cooperative project by ESA and NASA to study the Sun, from its deep core to the outer corona, and the solar wind. It carries a complement of twelve sophisticated instruments (Table 1) developed and furnished by twelve international Principal Investigator (PI) consortia involving 39 institutes from fifteen countries (Belgium, Denmark, Finland, France, Germany, Ireland, Italy, Japan, The Netherlands, Norway, Russia, Spain, Switzerland, United Kingdom, and the United States). Detailed descriptions of all twelve instruments, the science operations and data products, as well as a complete mission overview, can be found in ESA Bulletin No. 87.

SOHO has a unique operating mode that provides a 'live' display of data on the scientists' work stations in the SOHO Experimenters' Operations Facility (EOF) at NASA/Goddard Space Flight Center, from where they can command their instruments in near real time. From the outset SOHO was conceived as an integrated package of complementary instruments, being once described as an 'object-oriented, rather than an instrument-oriented mission'. There is therefore great emphasis on coordinated observations. Internally, this is facilitated through a nested scheme of planning meetings (monthly, weekly, daily), and externally through close coordination and data exchange for special campaigns and collaborations with other space missions and ground-based observatories over the Internet.

More than 500 articles have already appeared in the refereed literature and over 1500 articles in conference proceedings and in other publications. Here, we can only touch upon some selected highlights.

Global structure and dynamics of the solar interior

Just as seismology reveals the Earth's interior by studying earthquake waves, solar physicists probe the inside of the Sun using a technique called 'helioseismology'. The oscillations detectable at the visible surface are due to sound waves reverberating through the Sun's interior. These oscillations are usually described in terms of normal modes (identified by three integers: angular degree l, angular order m, and radial order n). The frequencies of the modes depend on the structure and flows in the regions where they propagate. Because different modes sample different regions inside the Sun, one can, in principle, map the solar interior by observing many modes. By measuring precisely the mode frequencies, one

Table 1. The SOHO scientific instruments

	Investigation	Principal Investigator
GOLF	Global Oscillations at Low Frequencies	A. Gabriel, IAS, Orsay, France
VIRGO	Variability of Solar Irradiance and Gravity Oscillations	C. Fröhlich, PMOD Davos, Switzerland
MDI	Michelson Doppler Imager	P. Scherrer, Stanford University, USA
SUMER	Solar Ultraviolet Measurements of Emitted Radiation	K. Wilhelm, MPAe Lindau, Germany
CDS	Coronal Diagnostic Spectrometer	R. Harrison, RAL, Chilton, UK
EIT	Extreme-Ultraviolet Imaging Telescope	J.-P. Delaboudinière, IAS, Orsay, France
UVCS	Ultra-Violet Coronagraph Spectrometer	J. Kohl, SAO, Cambridge, USA
LASCO	Large-Angle Spectroscopic Coronagraph	R. Howard, NRL, Washington, USA
SWAN	Solar Wind Anisotropies	J.-L. Bertaux, SA, Verrières, France
CELIAS	Charge, Element and Isotope Analysis System	P. Bochsler, Univ. of Bern, Switzerland
COSTEP	Comprehensive Supra-Thermal and Energetic-Particle Analyser	H. Kunow, Univ. of Kiel, Germany
ERNE	Energetic and Relativistic Nuclei and Electron Experiment	J. Torsti, Univ. of Turku, Finland

IAS : Institut d'Astrophysique Spatiale
PMOD : Physikalisch-Meteorologisches Observatorium Davos
RAL : Rutherford Appleton Laboratory
MPAe: Max-Planck-Institut für Aeronomie
SAO : Smithsonian Astrophysical Observatory
NRL : Naval Research Laboratory
SA : Service d'Aeronomie

can infer the temperature, density, elemental and isotopic abundances, interior mixing, interior rotation and flows, even the age of the Solar System, and pursue such esoteric matters as testing the constancy of the gravitational constant.

Interior rotation and flows

The nearly uninterrupted data from SOHO's Michelson Doppler Imager (MDI) yield oscillation power spectra with an unprecedented signal-to-noise ratio that allow the determination of the frequency splittings of the global resonant acoustic modes of the Sun with exceptional accuracy. These data confirm that the decrease in angular velocity Ω with latitude seen at the surface extends with little radial variation through much of the convection zone, at the base of which is an adjustment layer, called the 'tachocline', leading to nearly uniform rotation deeper in the radiative interior (Fig. 1). Furthermore, a prominent rotational shearing layer in which Ω increases just below the surface is discernible at low- to mid-latitudes.

The MDI team has also been able to study the solar rotation closer to the poles than has been achieved in previous investigations. The data have revealed that the angular velocity is distinctly lower at high latitudes than previously extrapolated from measurements at lower latitudes based on surface Doppler observations and helioseismology. Moreover, they found evidence of a submerged polar jet near latitudes of 75°, which is rotating more rapidly than its immediate surroundings (red oval near the poles in Fig. 2).

Alternating zonal bands of faster and slower rotation (± 7 m/s) at a depth of 2 – 9 Mm appear to coincide with an evolving pattern of 'torsional oscillations' reported from earlier surface Doppler studies (Fig. 2). Clear evidence of the migration of these zonal flows towards the equator has been found, and a recent study has established that these banded flows are not merely a near-surface phenomenon. Rather, they extend downward at least 60 Mm (some 8% of the total solar radius) and thus are evident over a significant fraction of the nearly 200 Mm depth of the solar convection zone (Fig. 3).

Long-lived velocity cells extending over 40–50° of longitude, but less than 10° of latitude, have been identified with the elusive 'giant cells' by Beck et al.. Their suprisingly large aspect ratio may be a consequence of the Sun's differential rotation, whereby larger features are broken up by rotational shear.

High-precision MDI measurements of the Sun's shape obtained during two special 360° roll manoeuvres of the SOHO spacecraft have

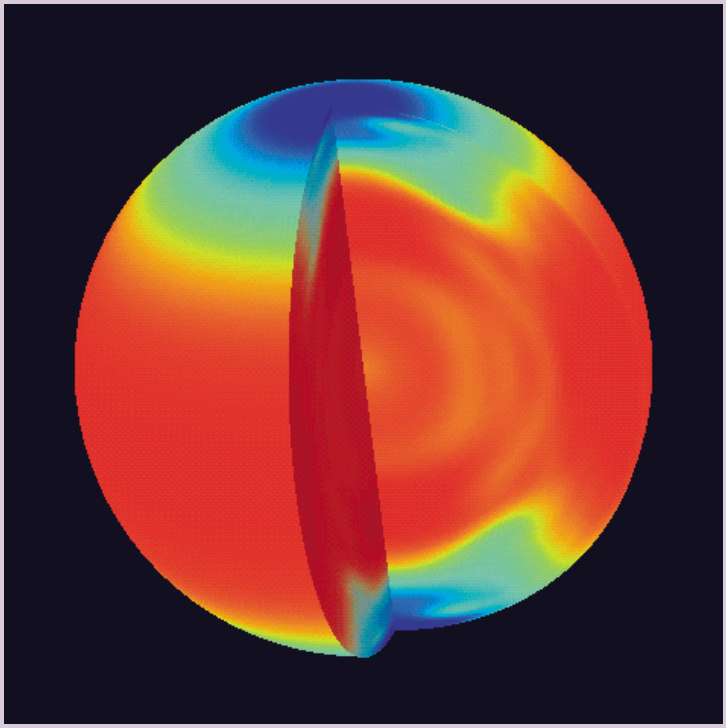

Figure 1. Solar interior rotation. Red indicates the fastest rotating material, dark blue the slowest (courtesy of SOHO/MDI Consortium)

Figure 2. Variations in solar motion. This false-colour image represents the difference in speeds between various areas on the Sun, both at the surface and in the interior. Red - yellow is faster and blue slower than average. On the left side of the image, the light-yellow bands are zones that are moving slightly faster than their surroundings. The cutaway on the right side of the image reveals speed variations in the interior of the Sun. Only the outer 30% of the Sun's interior where the variations are more certain is shown. The red ovals embedded in the green areas at the poles are the newly discovered polar plasma 'jet streams'. They move approximately 10% faster than their surroundings, and each is about 25 000 km across, large enough to engulf two Earths (courtesy of SOHO/MDI Consortium)

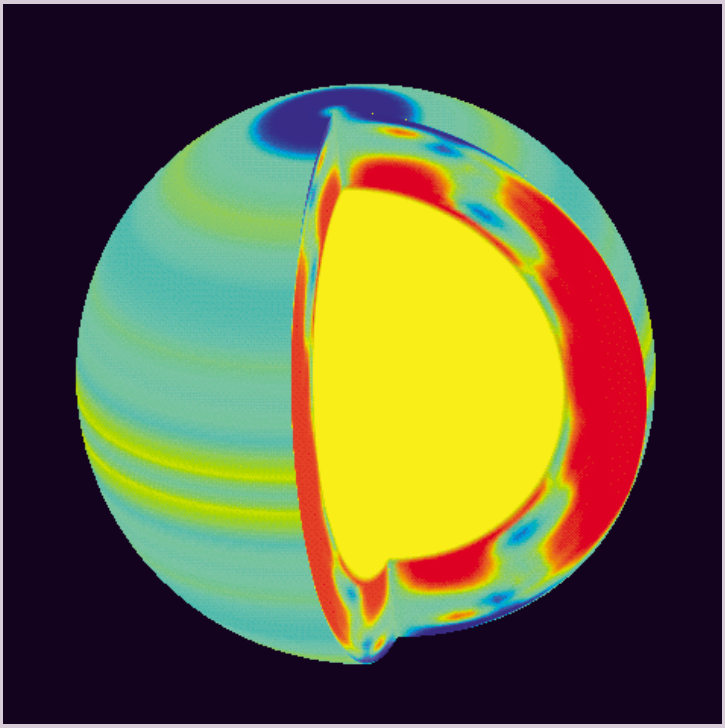

Figure 3. Migrating banded zonal flows: variation of rotation rate with latitude and time at four different depths in the convection zone. The uniform olive-green vertical bands indicated time periods when no data were available from SOHO (during the summer of 1998 due to the temporary loss of the spacecraft, and in January 1999 when SOHO was in safe mode after a gyroscope failure). The colour bar indicates the dynamic range in nHz of the angular velocity (from Howe et al.)

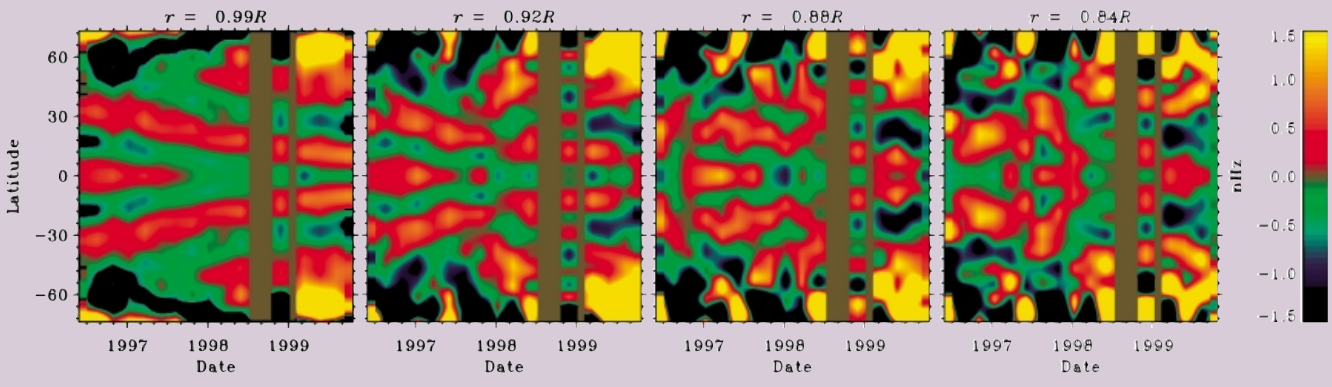

produced the most precise determination of solar oblateness ever. These measurements unambiguously rule out the possibility of a rapidly rotating core, and any significant solar-cycle variation in the oblateness.

Interior sound-speed profile

The unprecedented accuracy of helioseismic data from SOHO's MDI, GOLF and VIRGO instruments has enabled substantial improvements in models of the solar interior, and has even shown the importance of considering mixing effects, which turn out to solve existing riddles in the isotopic composition of the Sun.

Figure 4 is quite remarkable in that there is very good agreement between the measured sound speed and the model throughout most of the solar interior. Except for the conspicuous bump at about 0.68 $R_\odot$ (the location of the transition from the radiative zone into the convection zone), the difference is less than 0.2%, suggesting that our understanding of the mean radial stratification of the Sun is reasonably accurate.

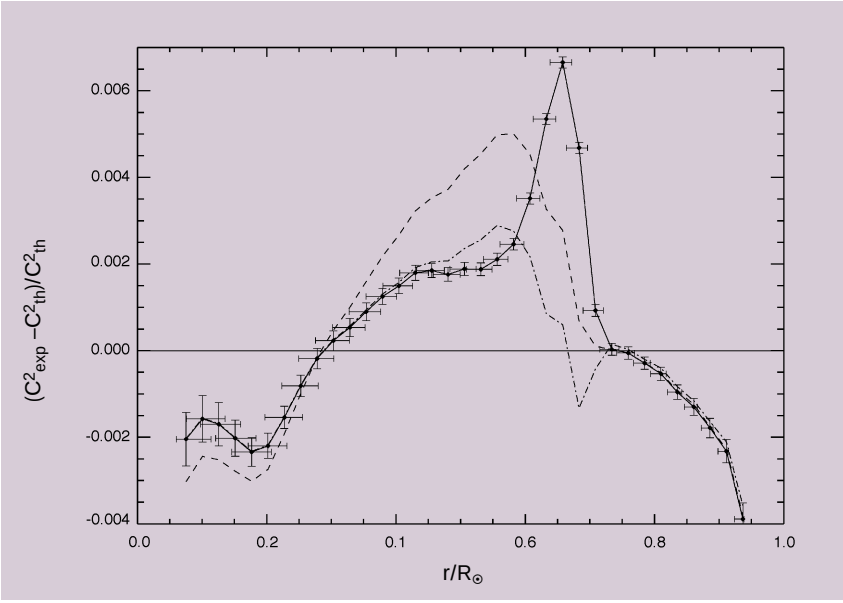

Figure 4. Relative differences between the squared sound speed in the Sun as observed by GOLF and MDI and a reference model (solid line), as well as two models including macroscopic mixing processes in the tachocline (dashed and dash-dotted lines) (from Brun et al.)

In order to resolve this discrepancy at 0.68 $R_\odot$ and the failure of recent updated standard models to predict the photospheric lithium abundance, Brun et al. introduced a new term – macroscopic mixing below the convective zone – into the standard stellar structure equations. They showed that the introduction of this 'tachocline layer mixing' significantly improves the agreement with the helioseismic data and photospheric abundance data. In particular, the anomalous bump in the sound-speed plot is practically erased (see the dash-dotted line in Fig. 4).

Local-area helioseismology

In conventional helioseismology, most results are obtained from a global-mode analysis. With the availability of high-spatial-resolution data from MDI, interest in studying the Sun's local structure has grown rapidly. As a result, several new techniques are being developed, including helioseismic holography, ring-diagram analysis and time-distance helioseismology.

Helioseismic holography

Originally proposed by Roddier in 1975 (though not as 'holography') and developed over the last few years mainly by Lindsey & Braun, this technique has been applied to MDI data to render acoustic images of the absorption and egression of sunspots and active regions. These images have revealed a remarkable acoustic anomaly surrounding sunspots, called the 'acoustic moat', which is a conspicuous halo of enhanced acoustic absorption at 3 mHz. At 5–6 mHz, on the other hand, a prominent halo of enhanced acoustic emission, called 'acoustic glory', was found surrounding active regions. Helioseismic holography techniques can be applied to render images of supposed acoustic sources that can be sampled at any desired depth. This technique has recently been applied by Lindsey & Braun to derive the first seismic images of the far side of the Sun, from MDI data (Fig. 5).

Ring-diagram analysis

The second technique, known as 'ring-diagram analysis', is based on the study of three-dimensional power spectra of solar p-modes on a part of the solar surface. Several groups have applied this technique to MDI data to determine near-surface flows in the Sun. A remarkable meridional flow from the equator to the poles was found in the outermost layers of the convection zone, reaching a maximum of 25–30 m/s at approximately 30° latitude. No change of sign of the meridional flow has been measured, i.e. no evidence of a return flow has been detected in this depth range. The rotation rate determined with the ring-diagram technique agrees well with that from global modes, and the measurements could be extended closer to the surface, providing new insight into the shear layer immediately beneath the surface.

Time-distance helioseismology

The third, and perhaps most exciting and most promising new technique for probing the three-dimensional structure and flows beneath the solar surface is called 'time-distance helioseismology' or 'solar tomography'. It measures the travel time of acoustic waves between various points on the surface. In a first-order approximation, the waves can be considered to follow ray paths that depend only on a mean solar model, with the curvature of the ray paths

being caused by the increasing sound speed with depth below the surface. The travel time is affected by various inhomogeneities along the ray path, including flow, temperature inhomogeneities, and magnetic fields. By measuring a large number of travel times between different locations and using an inversion method, it is possible to construct three-dimensional maps of the subsurface inhomogeneities.

By applying this new technique to high-resolution MDI data, Duvall et al. were able to generate the first maps of horizontal and vertical flow velocities as well as sound-speed variations in the convection zone just below the visible surface (Fig. 6). They found that in the upper layers, 2–3 Mm deep, the horizontal flow is organised in supergranular cells, with outflows from the cell centres. The characteristic size of these cells is 20–30 Mm and the cell boundaries coincide with the areas of enhanced magnetic field. The supergranulation outflow pattern disappears at a depth of approximately 5 Mm, suggesting that the depth of the supergranular layer is less than one quarter of the characteristic horizontal size of the cells (20–30 Mm).

One of the most successful applications of time-distance helioseismology has been the detection of large-scale meridional flows in the solar convection zone. Meridional flows from the equator to the poles have been observed before on the solar surface in direct Doppler-shift measurements. The time-distance measurements by the Stanford MDI team provided the first evidence that such flows

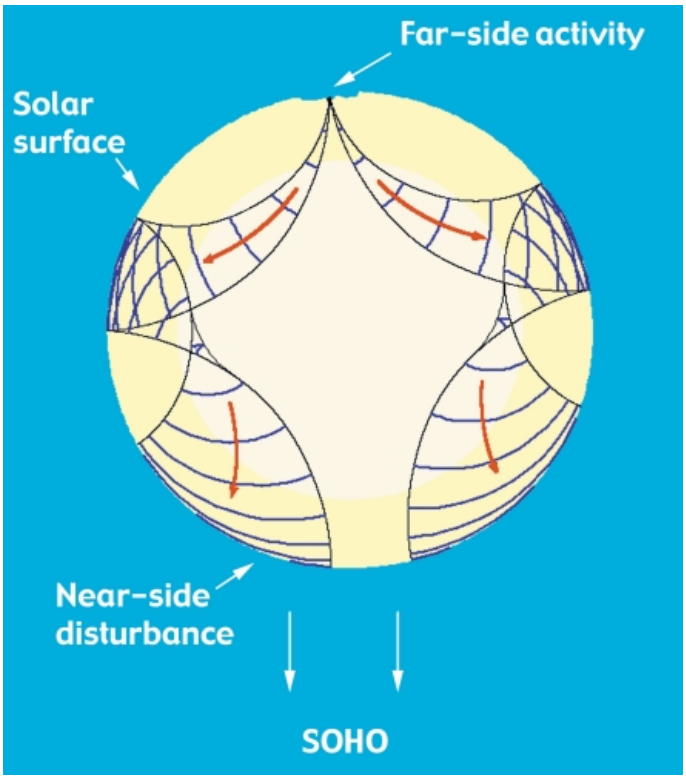

Figure 5a. Cross-section of the solar interior illustrating the wave configuration of two-skip far-side seismic holography. Sound waves from the far side of the Sun are reflected internally once before reaching the front side, where they are observed with MDI

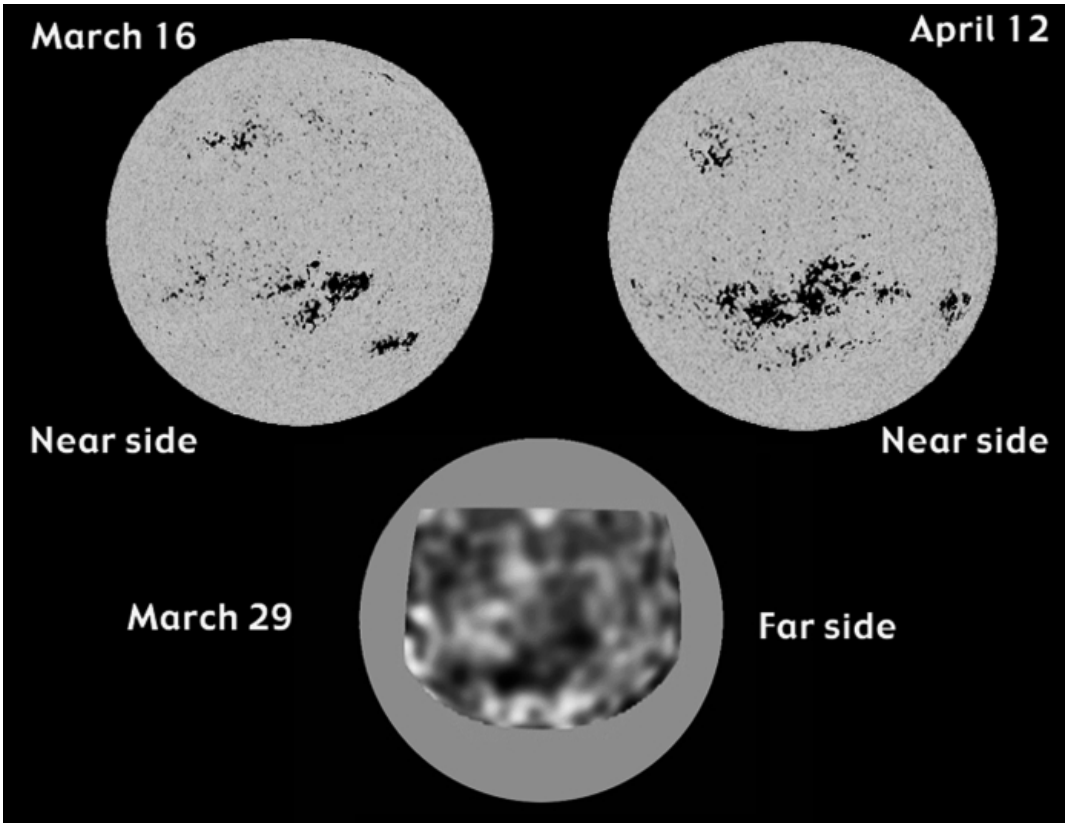

Figure 5b. The upper two images show the magnetic field strength measured with MDI while the active region was facing the Earth – before and after being holographically imaged on the far side, shown in the lower image (from Lindsey & Braun)

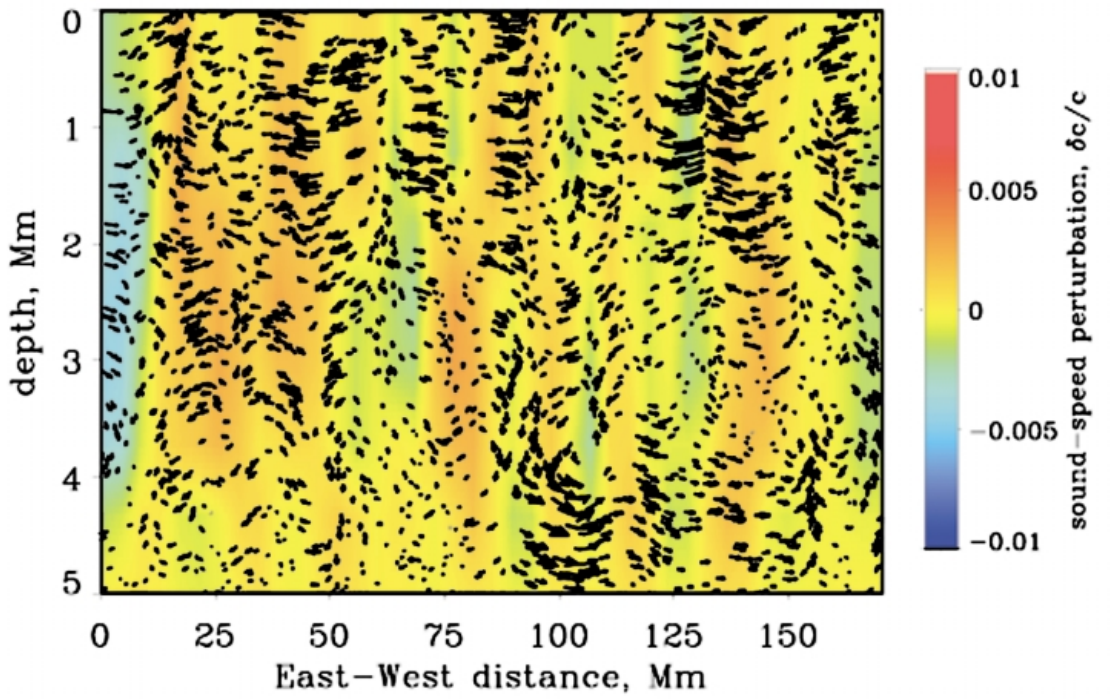

Figure 6. A vertical cut through the upper convection zone showing subsurface flows and sound speed inhomogeneities (from Kosovichev et al.)

persist to great depths (Fig. 7), and therefore may play an important role in the 11-year solar cycle. They found the meridional flow to persist to a depth of at least 26 Mm, with a depth-averaged velocity of 23.5 ± 0.6 m/s at mid-latitude. More recently, they extended these measurements to a depth of 0.8 $R_\odot$ without finding any evidence of a return flow. Continuity considerations led them to estimate the return flow below 0.8 $R_\odot$ at approximately 5 m/s, which might actually be detectable in the future, providing a useful constraint for dynamo theories.

One of the most exciting applications of solar tomography is in studying the birth and evolution of active regions and complexes of solar activity. Kosovichev et al. have studied the emergence of an active region on the Sun's disc with this technique and their results suggest that the emerging flux ropes travel very quickly through the upper 18 Mm of the convection zone. They estimate the speed of emergence at about 1.3 km/s, which is somewhat higher than predicted by earlier theories. Wave speeds vary in the emerging active region by about 0.5 km/s. The observed development of the active region suggests that the sunspots are formed as a result of the concentration of magnetic flux close to the surface. The Stanford team also presented time-distance results on the subsurface structure of a large sunspot observed on 20 June 1998 (Fig. 8). The wave-speed perturbations in the spot are much stronger than in the emerging flux (0.3–1 km/s). At a depth of 4 Mm, a 1 km/s wave-speed perturbation corresponds to a 10% temperature variation (approx. 2800 K) or to a 18 kG magnetic field. Beneath the spot, the perturbation is negative in the subsurface layers and becomes positive further down in the interior. Their tomographic images also revealed sunspot 'fingers' – long, narrow structures at a depth of about 4 Mm –

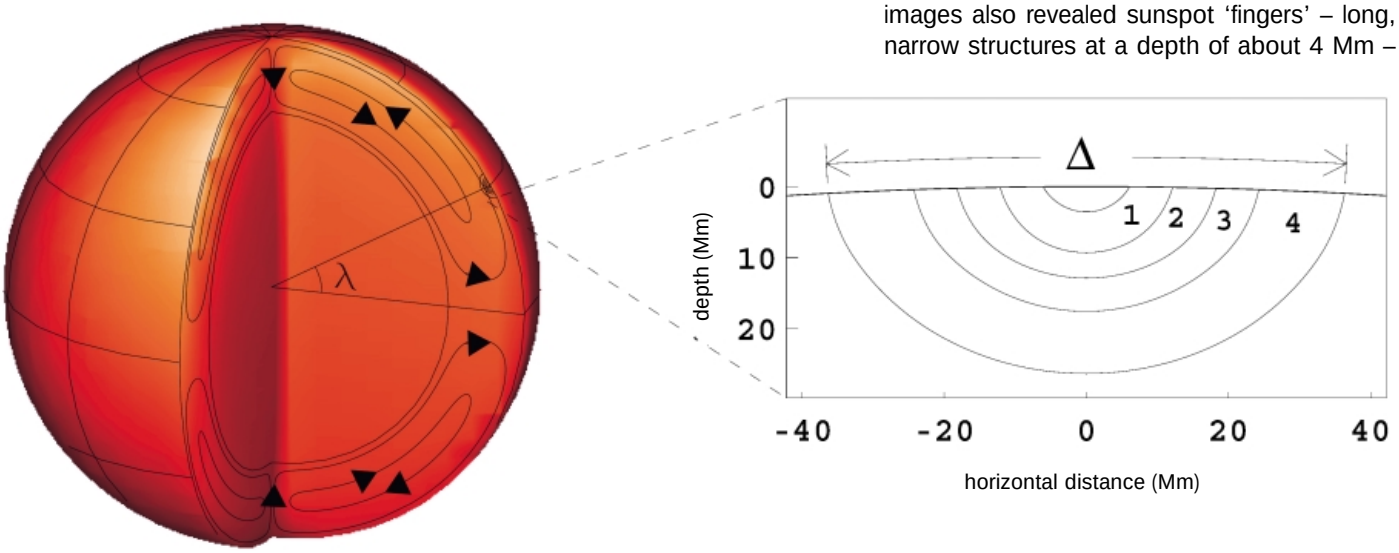

Figure 7. The geometry of the time-distance analysis of subsurface meridional flows (from Giles et al.)

which connect the sunspot with surrounding pores of the same polarity. Pores with the opposite polarity are not connected to the spot.

MDI has also made the first observations of seismic waves from a solar flare, opening up possibilities for studying both the flares and the solar interior. During the impulsive phase of the X2.6-class flare of 9 July 1996, a high-energy electron beam caused an explosive evaporation of chromospheric plasma at supersonic velocities. The upward motion was balanced by a downward recoil in the lower chromosphere, which excited propagating waves in the solar interior. On the surface, the outgoing circular flare waves resembled ripples from a pebble thrown into a pond (Fig. 9). The seismic wave propagated at least 120 000 km from the flare's epicentre, with an average speed of about 50 km/s on the solar surface.

Transition-region dynamics

Explosive events and 'blinkers'

Several types of transient events have been detected in the quiet Sun. High-velocity events in the solar transition region, also called 'explosive events', were first discovered in the early eighties based on ultraviolet observations with the High-Resolution Telescope-Spectrometer (HRTS) rocket payload. They have large velocity dispersions, approximately ±100 km/s, i.e. velocities are directed both towards and away from the observer causing a strong broadening of the spectral lines observed.

Explosive events have been studied extensively by a number of authors using SUMER data, and several results support the magnetic reconnection origin of these features. Innes et al. have reported explosive events that show spatially separated blue- and red-shifted jets and some that show transverse motion of blue and red shifts, as predicted if reconnection was the source (Fig. 10). Comparisons with magnetograms from MDI and those obtained at ground-based solar observatories have also provided evidence that transition-region explosive events are a manifestation of magnetic reconnection occurring in the quiet Sun.

Harrison et al. have presented a comprehensive study of EUV flashes, also known as 'blinkers',

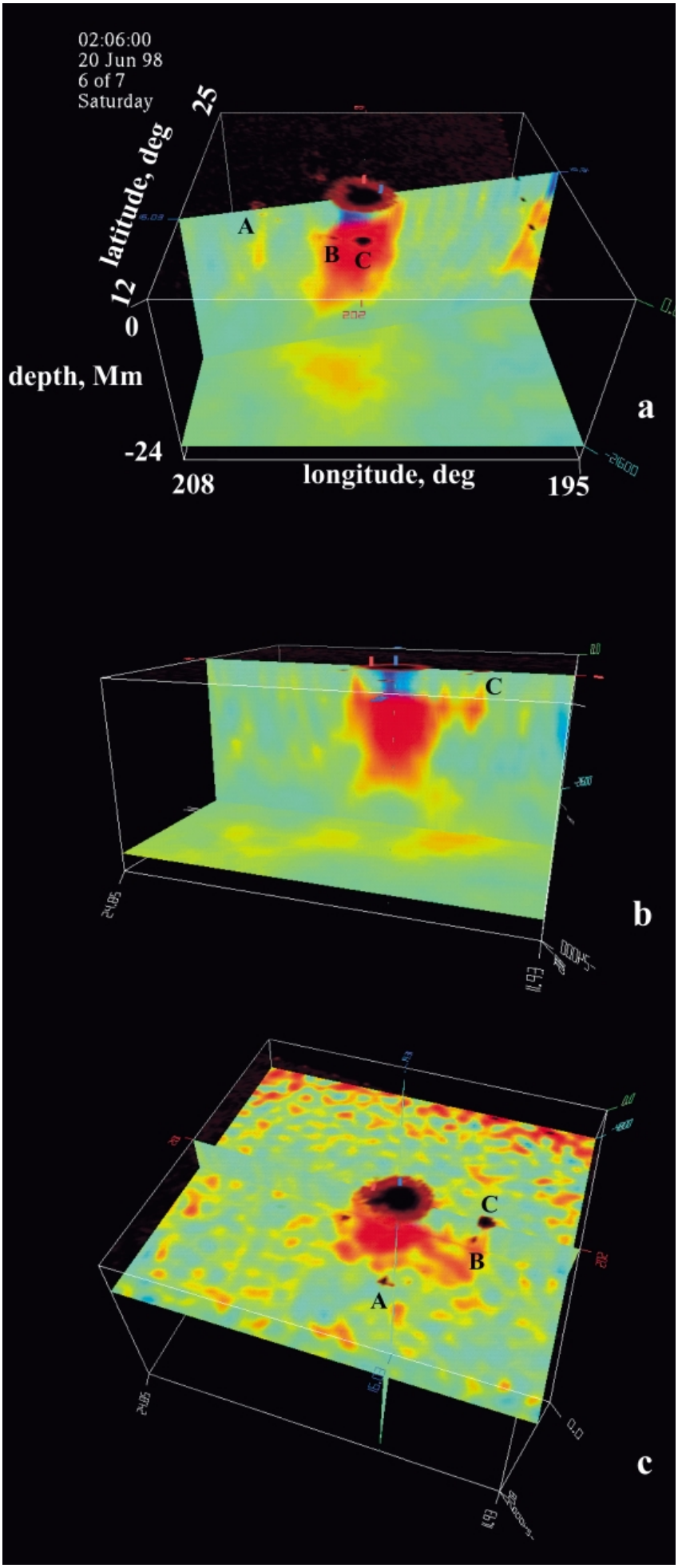

Figure 8. The subsurface sound speed perturbations in a sunspot region observed on 20 June 1998 by MDI. The horizontal size of the box is 13 deg (158 Mm), the depth is 24 Mm. The horizontal cut in panels (a) and (b) reaches down to a depth of 21.6 Mm, while in panel (c) it is 4.8 Mm deep. Positive variations are shown in red, negative variations in blue. Scaling: ±1 km/s (from Kosovichev et al.)

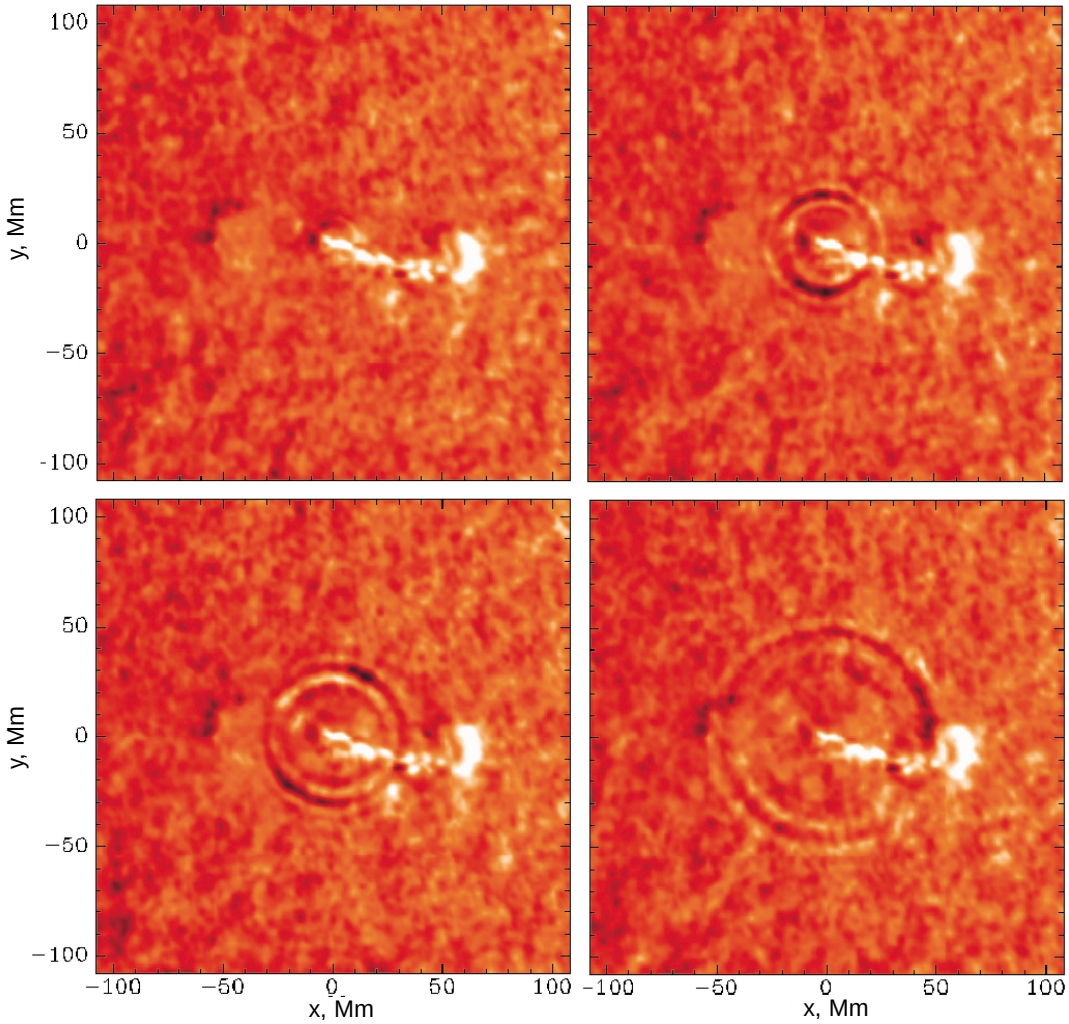

Figure 9. Seismic waves ('sun quake') produced by a solar flare on 9 July 1996 (from Kosovichev & Zharkova)

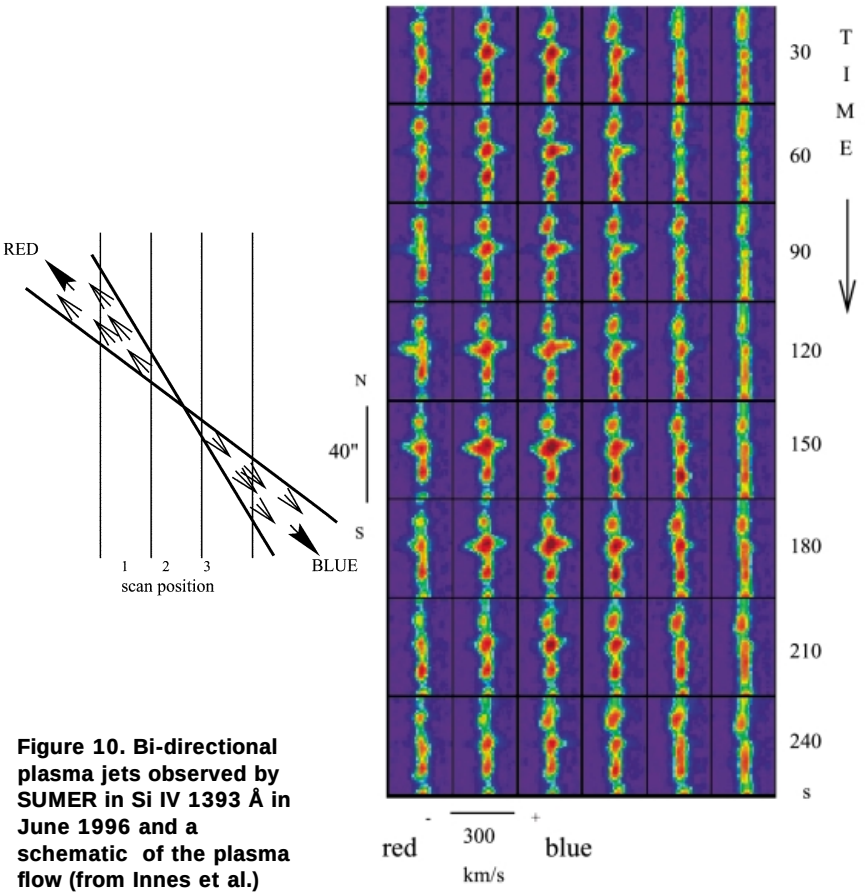

Figure 10. Bi-directional plasma jets observed by SUMER in Si IV 1393 Å in June 1996 and a schematic of the plasma flow (from Innes et al.)

which were identified in the quiet Sun network as intensity enhancements of order 10–40% using CDS (Fig. 11). They have analysed 97 blinker events and identified blinker spectral, temporal and spatial characteristics, their distribution, frequency and general properties, across a broad range of temperatures, from 20 000 to 1 200 000 K. The blinkers are most pronounced in the transition region lines O III, O IV and O V, with modest or no detectable signature at higher and lower temperatures. A typical blinker lasts about 1000 s, but due to a long tail of longer duration events the average duration is 2400 s. Comparisons with plasma cooling times led to the conclusion that there must be continuous energy input throughout the blinker event. There are about 3000 blinker events in progress at any given time. Remarkably, line ratios from O III, O IV and O V show no significant change throughout the blinker event, suggesting that the intensity increase is not a temperature effect, but is predominantly caused by increases in density or filling factor. The thermal-energy content of an average blinker is estimated as 2 x 10^{25} erg.

While the explosive events appear as extremely broad line profiles with Doppler shifts of

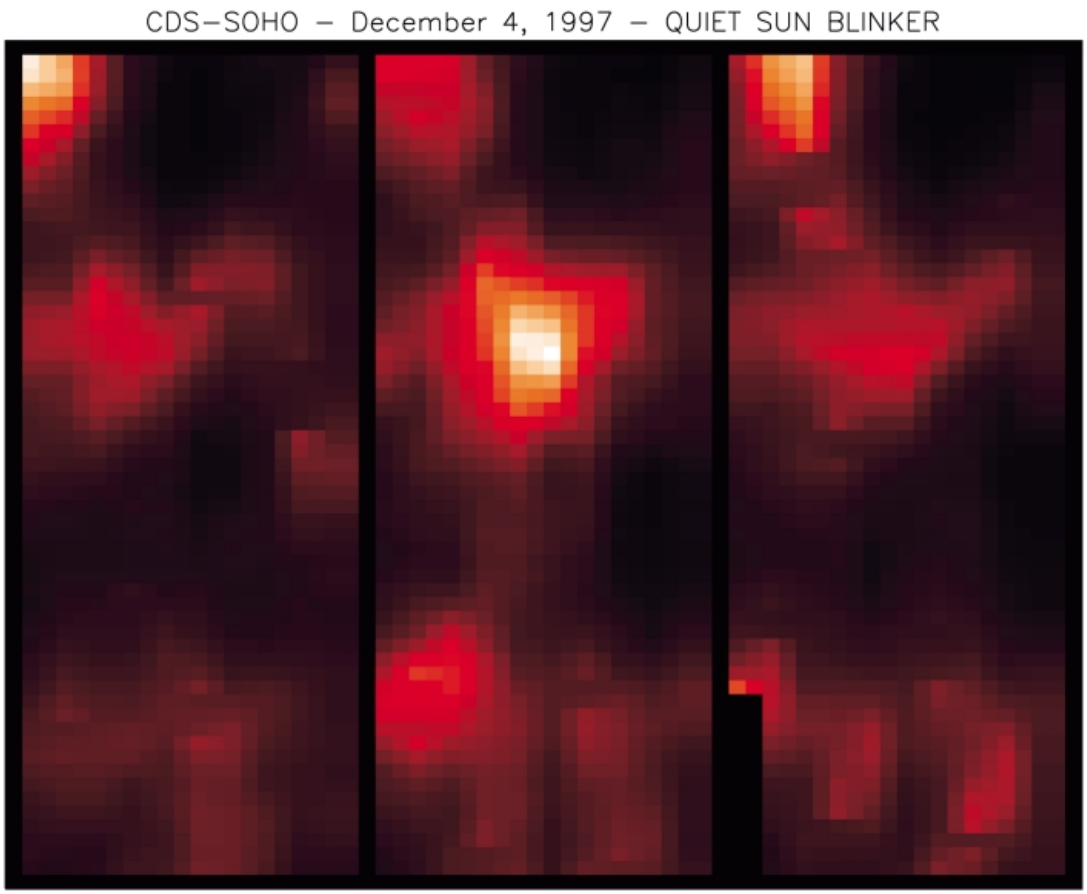

Figure 11. 'Blinker' event observed by CDS in OV 629 Å (T ≈ 230 000 K). The area shown covers 30 000 x 74 000 km². The three images are minutes apart (from Harrison et al.)

±150 km/s without significant brightenings, spectral-line fits to CDS data have so far revealed no clear velocity shifts, or only modest velocities up to a maximum of 20 km/s. Typically, the explosive events are short-lived (approx. 60 s), small scale (about 2 arcsec) and occur at a rate of 600 s^{-1} over the Sun's surface. While both types of event appear fairly common, they are seemingly of two different classes and further analysis is needed to establish the relationship between the two phenomena.

Doppler-shifted emission in the transition region

It has long been known that the UV emission lines originating from the transition region of the quiet Sun are systematically redshifted relative to the underlying chromosphere. In earlier investigations the magnitude of the redshift has been found to increase with temperature, reaching a maximum at T ≈ 10^5 K, and then to decrease sharply towards higher temperatures. Systematic redshifts have also been observed in stellar spectra of late-type stars, first with the International Ultraviolet Explorer (IUE) satellite and more recently with the Hubble Space Telescope. Below temperatures of about 1.6 x 10^5 K, the line redshifts of the Sun, α Cen A, α Cen B, and Procyon are all very similar.

Early SOHO observations extended the observable temperature range and suggested that the average redshift persists to higher temperatures than most previous investigations suggested. Shifts of 10 to 16 km/s were observed in lines formed at T=1.3–2.5 x 10^5 K (Fig. 12). Even upper transition region and coronal lines (O VI, Ne VIII, and Mg X) showed systematic redshifts in the quiet Sun corresponding to velocities around 5 km/s.

Figure 12. Variation of the Doppler shift at disc centre with formation temperature of the line. The solid line is a by-eye fit to the Doppler shifts (from Peter & Judge)

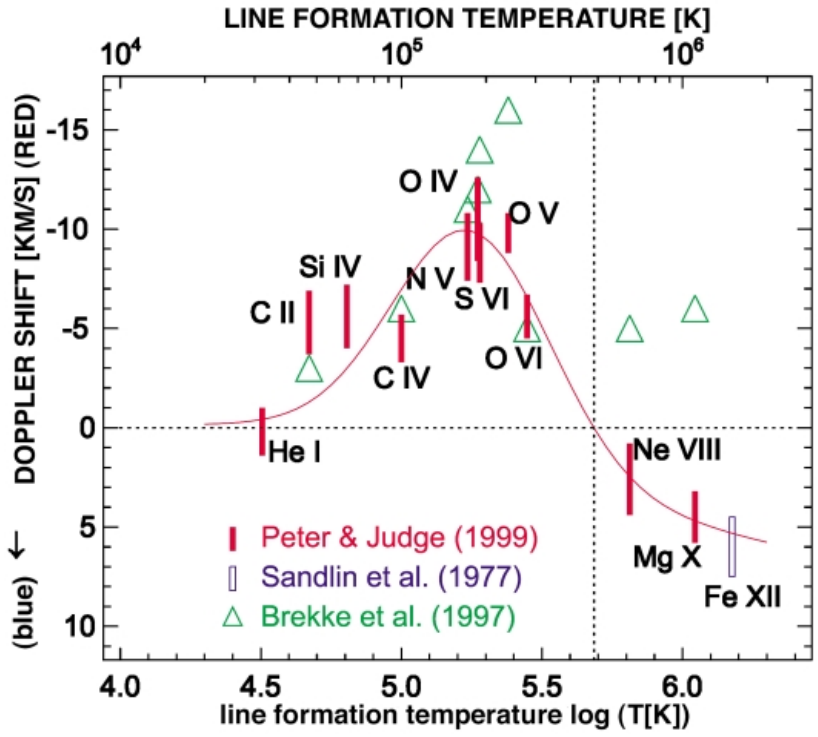

More recent investigations using SUMER observations have revisited this problem, addressing possible errors in the rest wavelengths of lines from highly ionised atoms (e.g. Ne VIII, Na IX, Mg X, Fe XII). Using full-disc scans from SUMER and assuming that all mass or wave-motion effects on the limb cancel out statistically, new rest wavelengths for Ne VIII and Mg X have been established, leading to blueshifts of 2.5 km/s and 4.5 km/s, respectively, at disc centre.

These recent results suggest that the upper transition region and lower corona appear blue-shifted in the quiet Sun, with a steep transition from red- to blue-shifts above 5 x 10^5 K. This transition is significant because it has major implications for the transition region and solar-wind modelling, as well as for our understanding of the structure of the solar atmosphere.

The network

Early models of the solar atmosphere assumed that the temperature structure of the upper atmosphere was continuous, with a thin transition region connecting the chromosphere with the corona. This depiction now appears too simplistic. Rather, it seems that the solar atmosphere consists of a hierarchy of isothermal, highly dynamic loop structures. Of particular interest in this context is the network, which is believed to be the backbone of the entire solar atmosphere and the basic channel of the energy responsible for heating the corona and accelerating the solar wind.

Patsourakos et al. have used CDS data to study the width variation of the network with temperature. They found that the network boundaries have an almost constant width up to about 250 000 K (where the network contrast is also strongest) and then fan out rapidly at coronal temperatures. The network in the lower transition region is about 10 arcsec across and spreads to about 16 arcsec at 1 MK. These results are in very good agreement with Gabriel's transition region-corona model, dating from1976.

Active-region dynamics

EIT, SUMER and CDS observations have clearly demonstrated that the solar transition region and corona are extremely dynamic and time variable in nature. Large line shifts of up to 60 km/s were observed with CDS in individual active region loops (Fig. 13). High Doppler shifts are common in active-region loops and strong shifts are present in parts of loops for temperatures up to 0.5 MK. Regions with both red and blue shifts are seen. While typical values correspond to velocities of ± 50-100 km/s, shifts approaching 200 km/s have been detected. At temperatures T > 1 MK, i.e. in Mg IX 368 Å or Fe XVI 360 Å, only small shifts are seen. The high Doppler shifts therefore seem to be restricted to the transition region.

Brynildsen et al. studied 3-min transition-region oscillations above sunspots by analysing time series recorded in O V 629 Å, N V 1238 Å and 1242 Å, and the chromospheric Si II 1260 Å line in NOAA 8378. The 3-min oscillations that

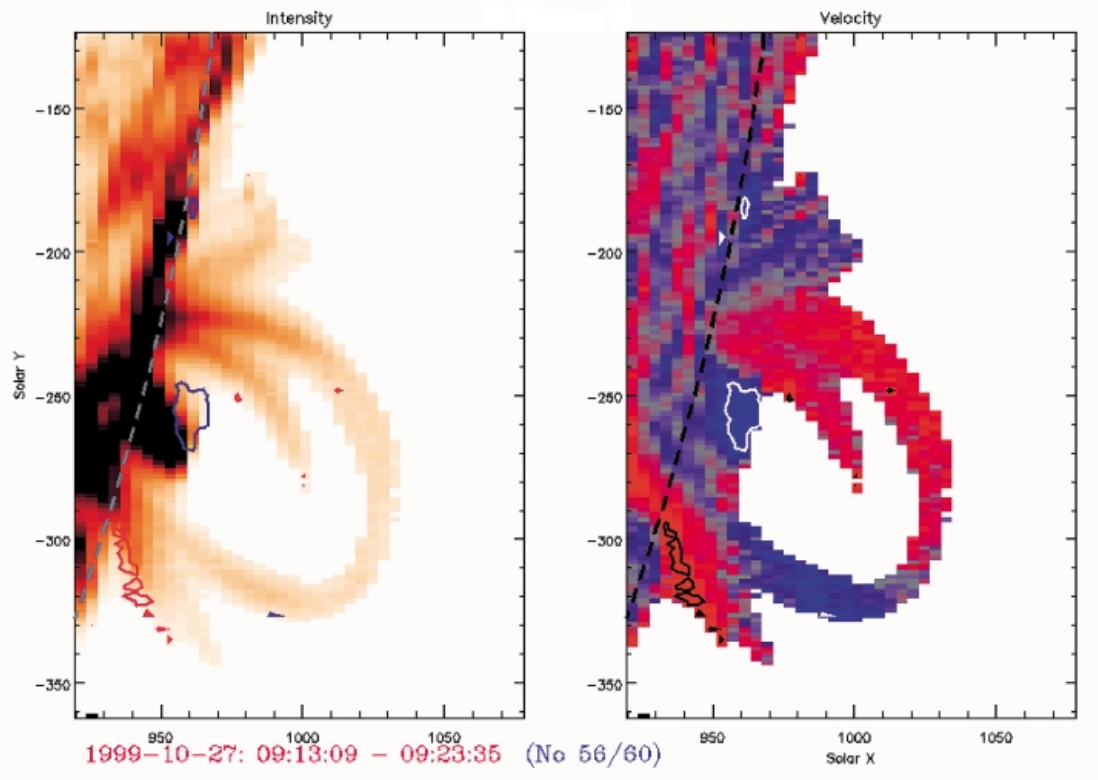

Figure 13. Coronal Diagnostic Spectrometer (CDS) raster images showing the intensity and velocity distribution of transition-region plasma in AR8737 on the south-west limb in October 1999. Six emission lines were observed simultaneously, of which one is shown here (O V 629 Å, formed at about 230 000 K). Doppler shifts corresponding to a velocity greater than ± 40 km/s (144 000 km/h) are fully red/blue. Contours outline areas with velocities exceeding ± 50 km/s (180 000 km/h) (courtesy of T. Fredvik & O. Kjeldseth-Moe)

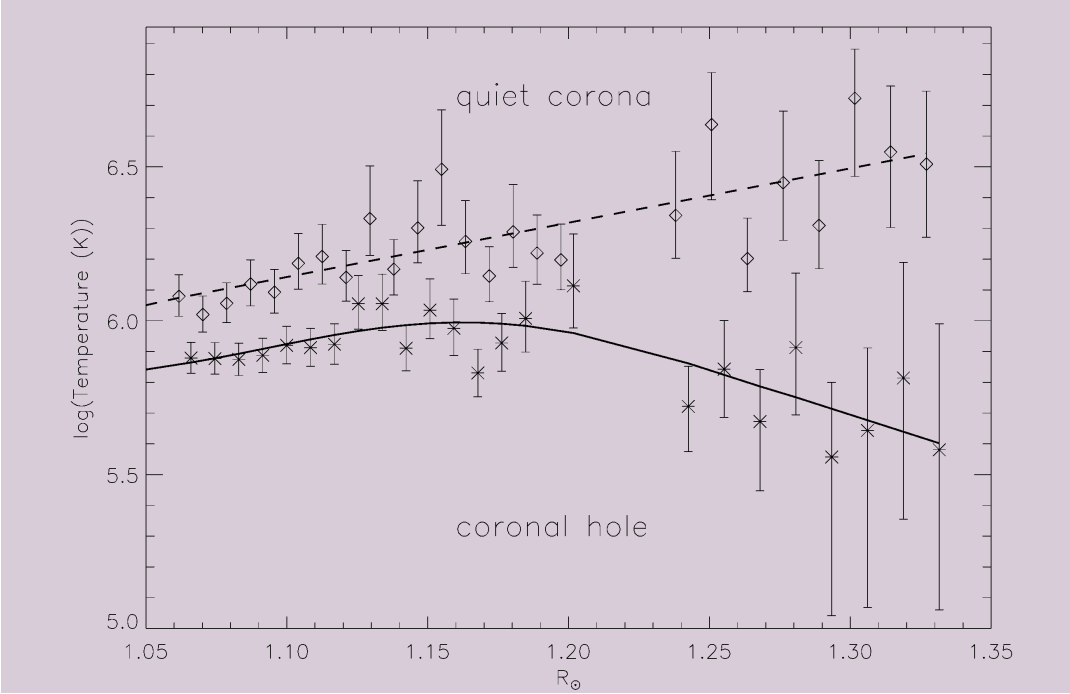

Figure 14. Temperature gradient measurement in the quiet corona (equatorial west limb) and the north polar coronal hole (from David et al.)

they observed above the sunspot umbra show: (a) larger peak line intensity amplitudes than reported previously, (b) clear signs of non-linearities, (c) significant oscillations in line width, and (d) maxima in peak line intensity and maxima in velocity directed towards the observer that are nearly in phase. They also performed a simple test and calculated the velocity oscillations from the intensity oscillations (which, to a first approximation for optically thin lines, is proportional to ρ^2) using a standard text-book equation for simple nonlinear acoustic waves. The agreement with the observed velocity is astounding, providing convincing evidence that the oscillations that they observed are upward-propagating, nonlinear acoustic waves.

Corona

Coronal-hole temperature and density measurements

Using the two SOHO spectrometers CDS and SUMER, David et al. have measured the electron temperature as a function of height above the limb in a polar coronal hole (Fig. 14). Temperatures of around 0.8 MK were found close to the limb, rising to a maximum of less than 1 MK at 1.15 $R_\odot$, then falling to around 0.4 MK at 1.3 $R_\odot$. In equatorial streamers, on the other hand, the temperature was found to rise constantly with increasing distance, from about 1 MK close to the limb to over 3 MK at 1.3 $R_\odot$. With these low temperatures, the classical Parker mechanism for solar-wind acceleration cannot alone explain the high wind velocities, which must therefore be due to the direct transfer of momentum from MHD waves to the ambient plasma.

One of the most surprising results from SOHO has been the extremely broad coronal profiles of highliy ionised elements such as oxygen and magnesium (Fig. 15). Kohl et al. and Cranmer et al. have presented a self-consistent empirical model of a polar coronal hole near solar minimum, based on H I and O VI UVCS spectroscopic observations. Their model describes the

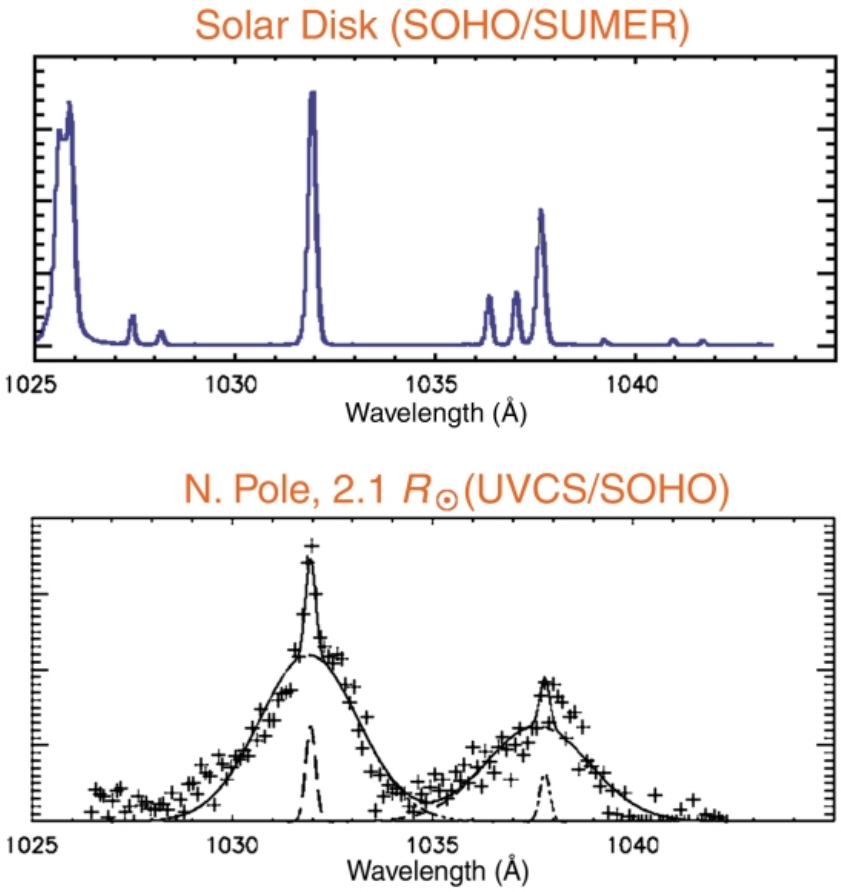

Figure 15. Line profile of O VI from UVCS observations in a polar coronal hole (lower panel) compared to disc observations from SUMER. The broad O VI line widths indicate velocities of up to 500 km/s, equivalent to a thermal-motion kinetic temperature of 200 million K. Narrow peaks in the lower panel are due to stray light (from Kohl et al.)

radial and latitudinal distributions of the density of electrons, H I and O VI, as well as the outflow velocity and unresolved anisotropic most probable velocities for H I and O VI.

Polar plumes

Wilhelm et al. have determined the electron temperatures, densities and ion velocities in plumes and interplume regions of polar coronal holes from SUMER spectroscopic observations of the Mg IX 706/750 Å and Si VIII 1440/1445 Å line pairs. They find the electron temperature T_e to be less than 800 000 K in a plume in the range from r = 1.03 to 1.60 $R_\odot$, decreasing with height to about 330 000 K. In the interplume lanes, the electron temperature is also low, but stays between 750 000 and 880 000 K in the same height interval. Doppler widths of O VI lines are narrower in the plumes ($v_{1/e} \approx 43$ km/s) than in the interplumes ($v_{1/e} \approx 55$ km/s). Thermal and turbulent ion speeds of Si VIII reach values up to 80 km/s, corresponding to a kinetic ion temperature of 10^7 K.

These results clearly confirm that the ions in a coronal hole are extremely hot and the electrons much cooler. They also clearly demonstrate that local thermal equilibrium does not exist in polar coronal holes, and that the assumption of Collisional Ionisation Equilibrium (CIE) and the common notion that $T_e \approx T_{ion}$ can no longer be made in models of coronal holes.

It seems difficult to reconcile these low electron temperatures measured in coronal holes with the freezing-in temperatures deduced from ionic charge composition data. The freezing-in concept, however, assumes that the adjacent charge states are in ionisation equilibrium. A critical reevaluation of this concept appears to be justified.

Previously, plumes were considered to be the source regions for the high-speed solar wind. Given the narrower line widths in plumes and the absence of any significant motions there, Wilhelm et al. suggested that the source regions of the fast solar wind are the interplume lanes rather than the plumes, since conditions there are far more suitable for a strong acceleration than those prevailing in plumes.

Heating processes

A promising theoretical explanation for the high temperatures of heavy ions and their strong velocity anisotropies is the efficient dissipation of high-frequency waves that are resonant with ion-cyclotron Larmor motions about the coronal magnetic-field lines. This effect has been studied in detail by Cranmer et al., who have constructed theoretical models of the non-equilibrium plasma state of the polar solar corona using empirical ion velocity distributions derived from UVCS and SUMER. They found that the dissipation of relatively small-amplitude high-frequency Alfvén waves (10–10 000 Hz) via gyro resonance with ion cyclotron Larmor motions can explain many of the kinetic properties of the plasma, in particular the strong anisotropies, the greater than mass-proportional temperatures, and the faster outflow of heavy ions in the high-speed solar wind. Because different ions have different resonant frequencies, they receive different amounts of heating and acceleration as a function of radius, which is exactly what is required to understand the different features of the H I and O VI velocity distributions. Furthermore, because the ion-cyclotron wave dissipation is rapid, the extended heating seems to demand a constantly replenished population of waves over several solar radii. This suggests that the waves are generated gradually throughout the wind, rather than propagating up from the base of the corona.

In addition to measuring velocity and intensity oscillation, MDI also measures the line-of-sight component of the photospheric magnetic field. In long, uninterrupted MDI magnetogram series, a continuous flux emergence of small bipolar regions has been observed. Small magnetic bipolar flux elements are continually emerging at seemingly random locations. These elements are rapidly swept by granular and mesogranular flows to supergranular cell boundaries where they cancel and replace existing flux. The rate of flux generation of this 'magnetic carpet' (Fig. 16) is such that all of the flux is replaced in about 40 hours, with profound implications for coronal heating on the top side and questions of local field generation on the lower side of the photosphere. Estimates of the energy supplied to the corona by 'braiding' of large-scale coronal fields through small-scale flux replacement indicate that it is much larger than that associated with granular braiding.

Coronal Mass Ejections

LASCO has been collecting an extensive database for establishing the best statistics ever on coronal mass ejections (CMEs; Fig. 17) and their geomagnetic effects. St.Cyr et al. have reported the properties of all 841 CMEs observed by the LASCO C2 and C3 white-light coronagraphs from January 1996 through the SOHO mission interruption in June 1998 and compared those properties with previous observations by other instruments. The CME rate for solar-minimum conditions was slightly higher than had been reported for previous solar cycles, but both the rate and the

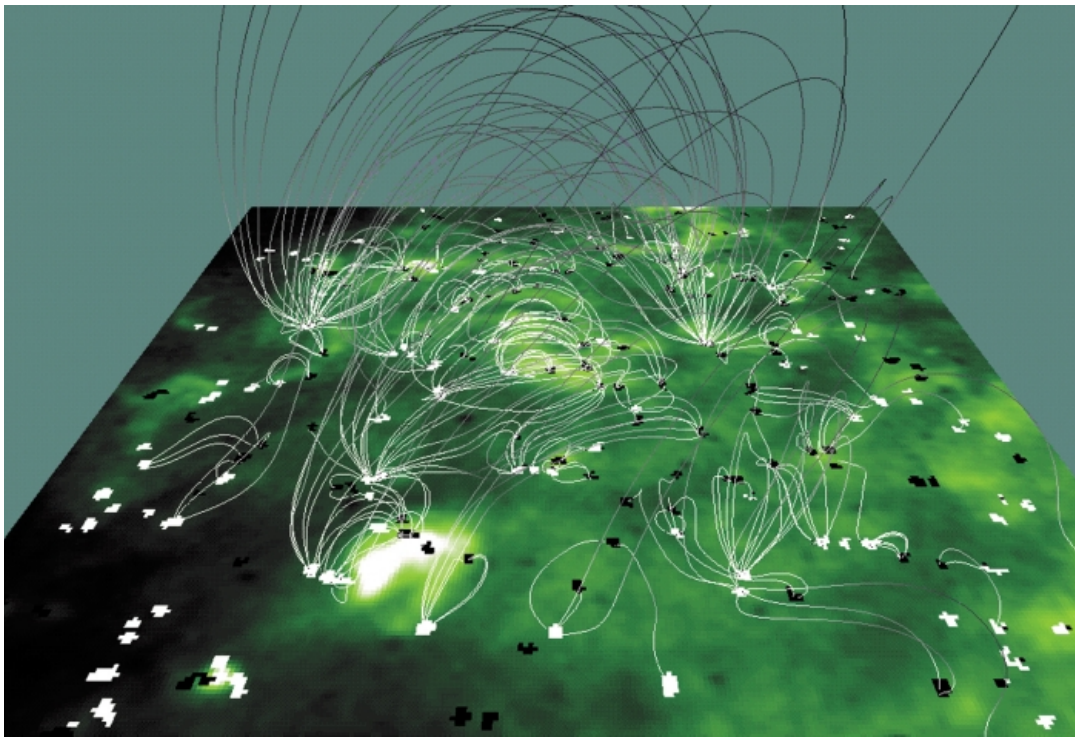

Figure 16. Magnetic carpet. Model of magnetic field lines based on MDI magnetograms, superimposed on an image of the solar corona in Fe XII 195 Å from EIT (courtesy of SOHO/MDI Consortium)

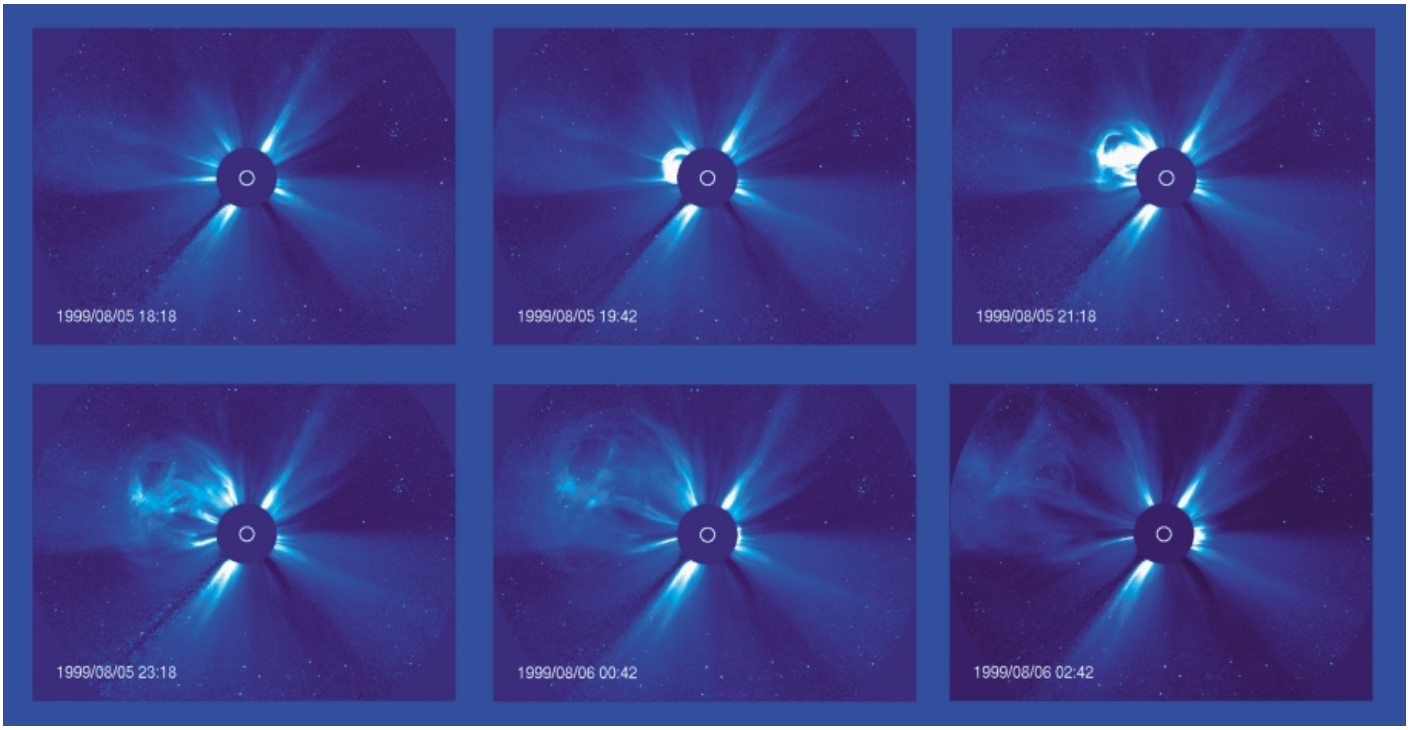

Figure 17. Progress of a Coronal Mass Ejection (CME) observed over an 8 h period on 5-6 August 1999 by LASCO C3. The dark disc blocks the Sun so that the LASCO instrument can observe the structures of the corona in visible light. The white circle represents the size and position of the Sun (courtesy of SOHO/LASCO Consortium)

distribution of apparent locations of CMEs varied during this period as expected. While the pointing stability provided by the SOHO platform in its L-1 orbit and the use of CCD detectors have resulted in superior brightness sensitivity for LASCO over earlier coronagraphs, they have not detected a significant population of fainter (i.e. low-mass) CMEs. The general shape of the distribution of apparent sizes for LASCO CMEs is similar to those of earlier reports, but the average (median) apparent size of 72° (vs. 50°) is significantly larger.

St.Cyr et al. have also reported on a population of CMEs with large apparent sizes, which appear to have a significant longitudinal component directed along the Sun–Earth line, either toward or away from the Earth. These are the so-called 'halo CMEs' (Fig. 18). Using full-disc EIT images, they found that 40 out of 92 of these events might have been directed towards the Earth. A comparison of the timing of those events with the Kp geomagnetic storm index in the days following the CME showed that 15 out of 21 (71%) of the Kp > 6 storms could be accounted for as SOHO LASCO/EIT front-side halo CMEs. Three more Kp storms may have

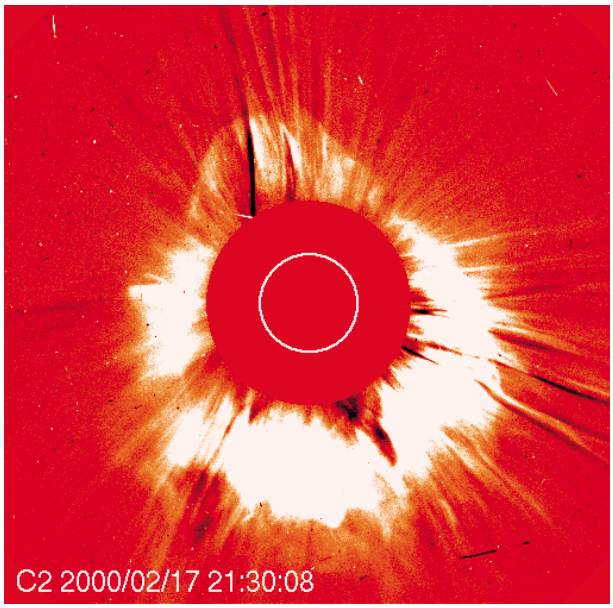

Figure 18. Massive 'halo' CME as recorded by LASCO C2 on 17 February 2000. Displayed here is a so-called 'running difference' image, showing the variation in brightness from one frame to the next (courtesy of SOHO/LASCO Consortium)

been missed during LASCO/EIT data gaps, bringing the possible association rate to 18 out of 21 (86%).

EIT has discovered large-scale transient waves in the corona, also called 'Coronal Moreton Waves' or 'EIT waves', propagating outward from active regions below CMEs. These events are usually recorded in the Fe XII 195 Å bandpass, during high-cadence (< 20 min) observations. Their appearance is stunning in that they usually affect most of the visible solar disc (Fig. 19). They generally propagate at speeds of 200–500 km/s, traversing a solar diameter in less than an hour. Active regions distort the waves locally, bending them towards the lower Alfvén speed regions. On the basis of speed and propagation characteristics, the EIT waves were associated with fast-mode shock waves. Another interesting aspect of these coronal Moreton waves is their association with the acceleration and injection of high-energy electrons and protons, as measured, for example, by COSTEP and ERNE.

Figure 19. Sequence of EIT difference images showing the intensity (density) enhancement and following rarefaction associated with a shock wave expanding across the solar disc from the site of the origin of a CME, recorded on 12 May 1997. A halo CME was observed by LASCO. These images were formed from the differences of successive images in the emission lines of Fe XII near 195 Å; this ion is formed at temperatures of about 1.5 million degrees. The wave front travels at speeds of ~ 300 km/s, typical of a fast mode Alfvén shock in the lower solar corona (from Thompson et al.)

Solar wind

Origin and speed profile of the fast wind

Coronal-hole outflow velocity maps obtained with the SUMER instrument in the Ne VIII emission line at 770 Å show a clear relationship between coronal-hole outflow velocity and the chromospheric network structure (Fig. 20), with the largest outflow velocities occurring along network boundaries and at the intersection of network boundaries. This can be considered the first direct spectroscopic determination of the source regions of the fast solar wind in coronal holes.

Proton and O VI outflow velocities in coronal holes have been measured by UVCS using the Doppler dimming method. The O VI outflow velocity was found to be significantly higher than the proton velocity, with a very steep increase between 1.5 and 2.5 $R_\odot$, reaching outflow velocities of 300 km/s at around 2 $R_\odot$ (Fig. 21). While the hydrogen outflow velocities are still consistent with some conventional theoretical models for polar wind acceleration, the higher oxygen flow speeds cannot be explained by these models. A possible explanation is offered by the dissipation of high-frequency Alfvén waves via gyroresonance with ion-cyclotron Larmor motions, which can heat and accelerate ions differently depending on their charge and mass.

Speed profile of the slow solar wind

Time-lapse sequences of LASCO white-light coronagraph images give the impression of a continuous outflow of material in the streamer belt. Density enhancements, or 'blobs', form near the cusps of helmet streamers and appear to be carried outward by the ambient solar wind. Sheeley et al., using data from the LASCO C2 and C3 coronagraphs, have traced a large number of such 'blobs' from 2 to over 25 solar radii. Assuming that these 'blobs' are carried away by the solar wind like leaves on

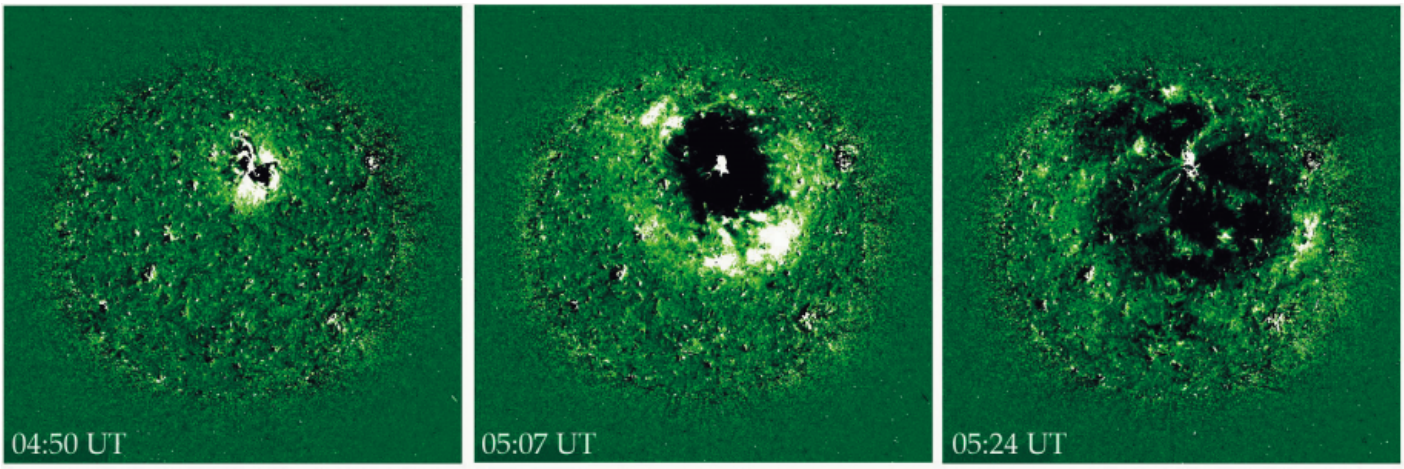

the river, they have measured the acceleration profile of the slow solar wind, which typically doubles its speed from 150 km/s near 5 $R_\odot$ to 300 km/s near 25 $R_\odot$. They found a constant acceleration of about 4 ms^{-2} through most of the 30 $R_\odot$ field-of-view. The speed profile is consistent with an iso-thermal solar-wind expansion at a temperature of about 1.1 MK and a sonic point near 5 $R_\odot$.

Solar-wind composition

Using data from the CELIAS/MTOF sensor, the CELIAS team has made the first in-situ determination of the isotopic composition of calcium and nitrogen in the solar wind. These measurements are important for studies of stellar modelling and Solar System formation, because the present-day solar Ca isotopic abundances are unchanged from their original isotopic composition in the solar nebula. The isotopic ratios $^{40}Ca/^{42}Ca$ and $^{40}Ca/^{44}Ca$ measured in the solar wind were found to be consistent with terrestrial values. The isotope ratio $^{14}N/^{15}N$ was found to be 200 ± 60, indicating a depletion of ^{15}N in the terrestrial atmosphere compared to solar matter.

Ion freeze-in temperatures were measured by CELIAS/CTOF with a time resolution of 5 min. These measurements indicate that some of the filamentary structures of the inner corona observed in H_α survive in the inter-planetary medium as far as 1 AU.

The unprecedented time resolution of the CELIAS/CTOF data has allowed a fine-scaled study of the elemental Fe/O ratio as a function of the solar-wind bulk speed. Since Fe is a low First Ionisation Potential (FIP) element and O a high-FIP element, their relative abundance is diagnostic for the so-called 'FIP fractionation process'. The Fe/O abundance shows a continuos decrease with increasing solar-wind speed by a factor of two between 350 km/s and 500 km/s, in correspondence with the well-established FIP effect.

Comets

SOHO is not only providing new measurements about the Sun. On 4 February 2000, SOHO discovered its 100th comet, 93 of which belong to the Sun-grazing Kreutz family (Fig. 22). A particular feature is the presence of a dust tail for only a few Sun grazers. Analysis of the light curves is used to investigate the properties of the nuclei (size, fragmentation, destruction) and the dust production rates.

Thanks to rapid communication from the LASCO group and the near-real-time observing capabilities of the SOHO instruments, UVCS could make spectroscopy measurements of

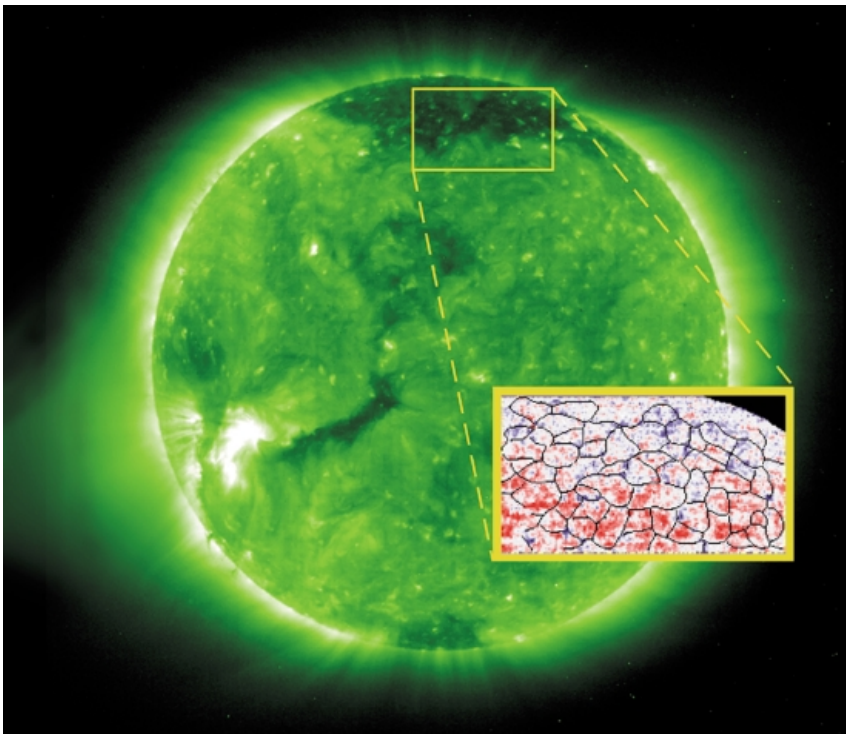

Figure 20. Source regions of the fast solar wind. Background: EIT full-Sun image taken in the emission line of Fe XII 195 Å, revealing gas at 1.5 million degrees shaped by magnetic fields. Bright regions indicate hot, dense plasma loops with strong magnetic fields, while dark regions imply an open magnetic field geometry, and are the source of the high-speed solar wind. The 'zoomed-in' or 'close-up' region shows a Doppler velocity map of plasma at about 630 000 K at the base of the corona, as recorded by SUMER in the Ne VIII emission line at 770 Å. Blue represents blue shifts or outflows and red represents red shifts or downflows. The blue regions are inside a coronal hole, or open magnetic field region, where the high-speed solar wind is accelerated. Superposed are the edges of 'honeycomb-shaped' patterns of magnetic fields at the surface of the Sun (from Hassler et al.)

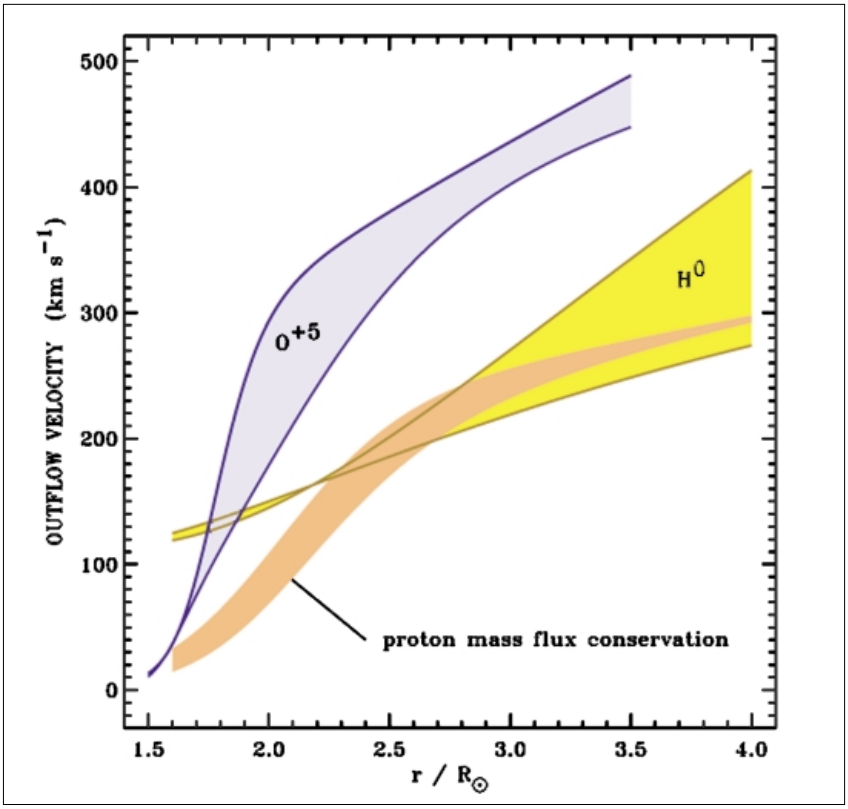

Figure 21. Empirical outflow velocity of O VI and H I in coronal holes over the poles (from Kohl et al.)

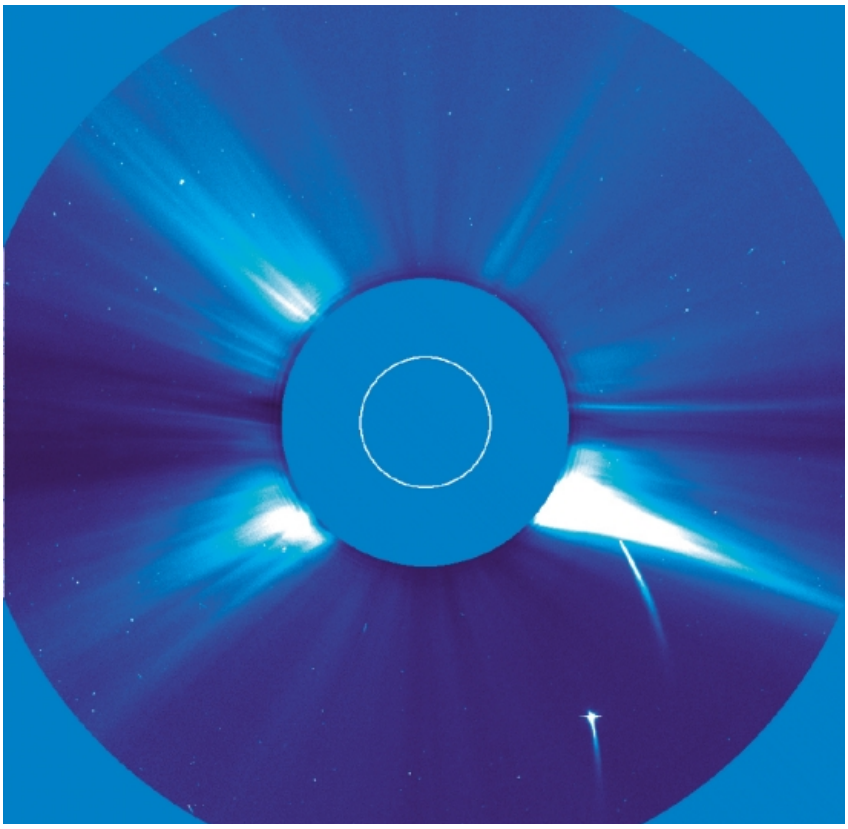

Figure 22. LASCO sees two comets plunge into the Sun. In a rare celestial spectacle, two comets were observed by the LASCO coronagraph plunging into the Sun's atmosphere in close succession, on 1 and 2 June 1998. Science instruments on SOHO have discovered more than 100 comets, including many so-called 'Sun grazers', but none in such close succession (courtesy of SOHO/LASCO Consortium)

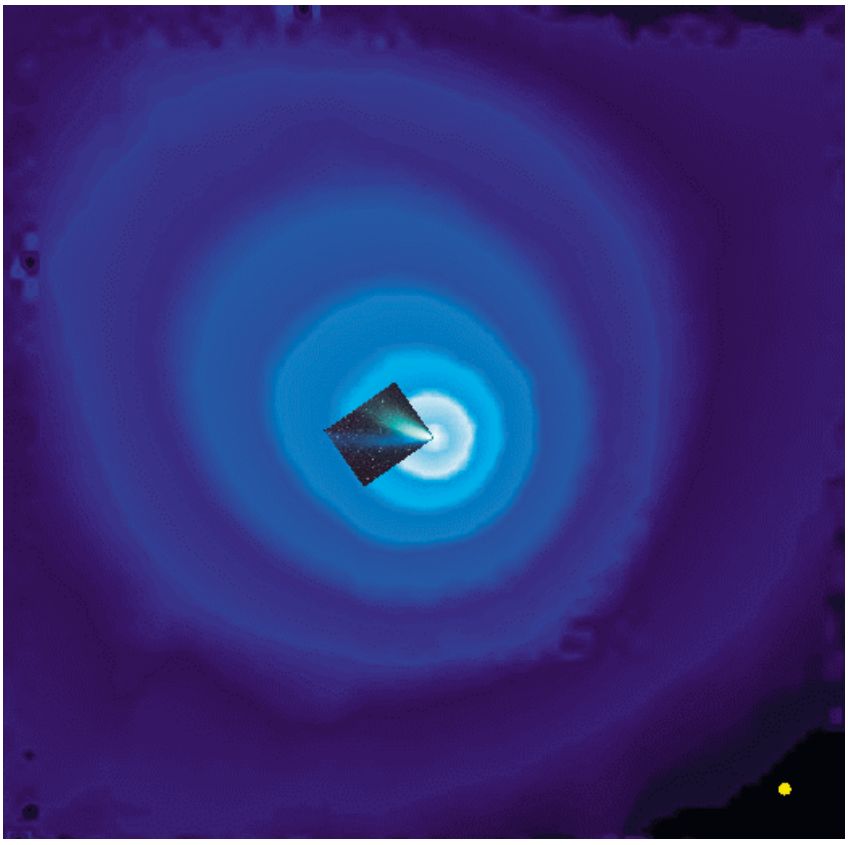

Figure 23. SWAN H I Ly-α image of the huge cloud of hydrogen surrounding comet Hale-Bopp when it neared the Sun in the spring of 1997. The small yellow dot shows the Sun to scale (from Combi et al.)

several comets on the day of their discovery. UVCS measurements of comet C/1996Y1 obtained at 6.8 $R_\odot$ confirmed the predictions of models of the cometary bow shock driven by mass-loading as cometary molecules are ionised and swept up in the solar wind. From the width and shift of the line profiles, the solar-wind speed at 6.8 $R_\odot$ could be determined (640 km/s). The outgassing rate of the comet was estimated at 20 kg/s, implying an active nucleus area of only about 6.7 m in diameter and a mass of about 120 000 kg.

Comets are surrounded by large clouds of hydrogen, produced by the break-up of water molecules evaporating from the comets' ice. The solar-wind mapper SWAN sees these large clouds of hydrogen glowing in the light of the H I Lyman-α line. The huge cloud of hydrogen surrounding Comet Hale-Bopp (Fig. 23) during its perihelion passage in the spring of 1997 was more than 100 million kilometres wide, diminishing in intensity outwards (contour lines). It far exceeded the great comet's visible tail (inset photograph). Although generated by a comet nucleus perhaps only 40 km in diameter, the hydrogen cloud was 70 times wider than the Sun itself (yellow dot to scale) and ten times wider than the hydrogen cloud of Comet Hyakutake observed by SWAN in 1996. The water evaporation rate of Hale-Bopp was measured by SWAN at more than 200 million tons per day. Comet Wirtanen, the target for ESA's Rosetta mission (2003), pumped out water vapour at a rate of 20 000 tons a day during its most recent periodic visit to the Sun, according to the SWAN data. SWAN has also seen something else extraordinary – the biggest shadow ever observed in our Solar System, namely that of a comet projected on the sky behind it (Fig. 24).

Heliosphere

The Sun is moving through the Local Interstellar Cloud (LIC) at about 26 km/s. The solar wind builds a cavity, the heliosphere, within the ionised gas component of the LIC. The neutral atoms (e.g. He) of the LIC, on the other hand, enter the heliosphere unaffected. The He flow properties are now well-constrained from a series of measurements (v_{He} = 25.5 ± 0.5 km/s, T_{He} = 6000 ± 1000 K). These values are in agreement with the LIC velocity and temperature deduced from stellar spectroscopy. Hydrogen, on the other hand, is expected to be affected by coupling with the decelerated plasma via charge-exchange. Neutral hydrogen heating and deceleration therefore provides a measurement of this coupling and, in turn, of the plasma density in the LIC, which is responsible for most of the heliosphere's confinement.

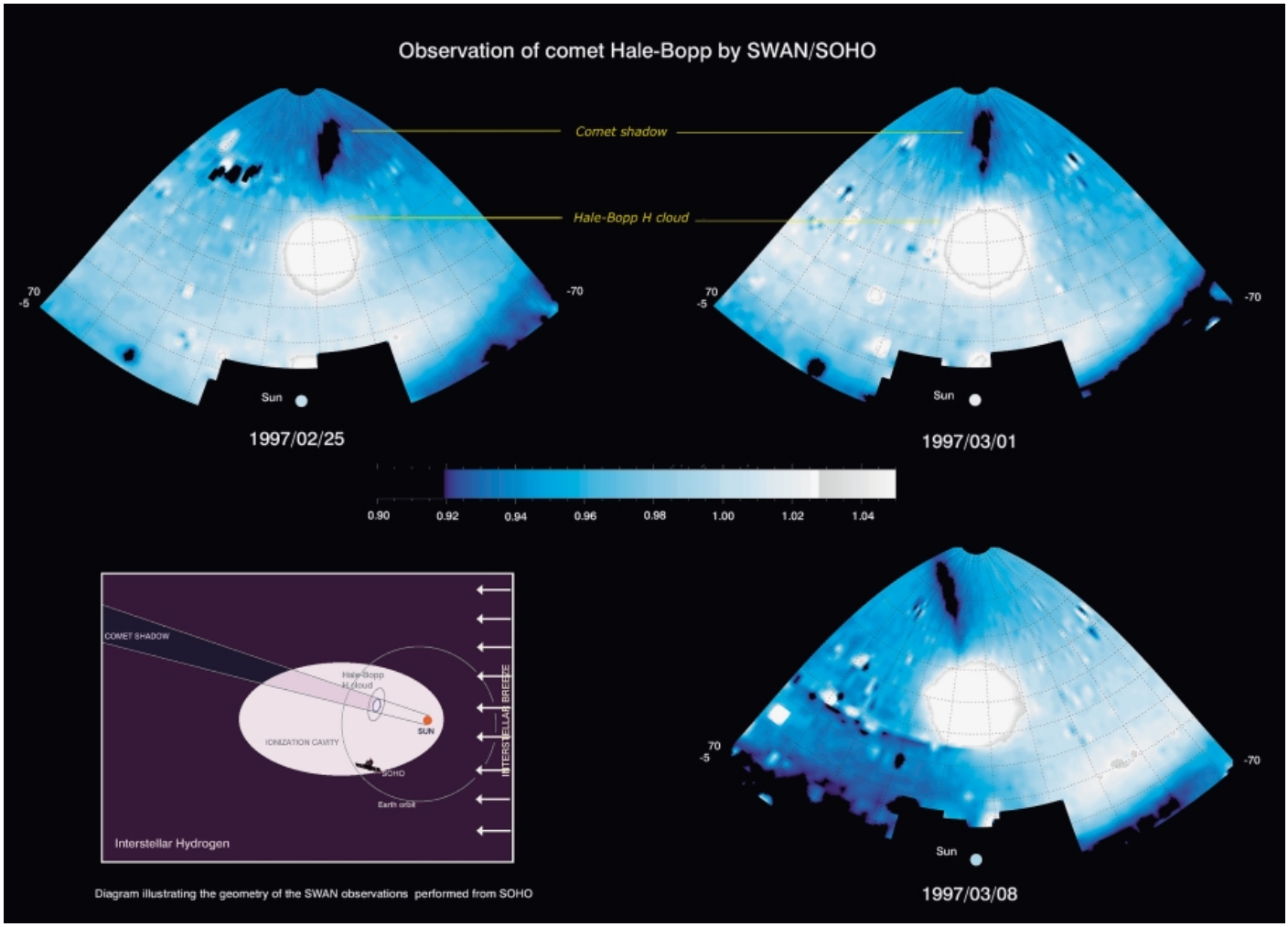

Figure 24. SWAN observations of comet Hale-Bopp's shadow (courtesy of SOHO/SWAN Consortium)

The SWAN team, analysing data from absorption cells, found hydrogen temperatures T_0 of 11 500 ± 1500 K, i.e. significantly above the temperature of the interstellar He flow (6000 ± 1000 K), requiring strong heating of more than 3500 K at the heliosphere interface. Part of this excess temperature is probably due to radiative-transfer effects.

The apparent interstellar hydrogen velocity in the up- and downwind direction was measured to be -25.4 ±1 km/s and +21.6 ±1.3 km/s, respectively, with the most precise determination (since model-independent) of the H flow direction. The new estimate of the upwind direction from SWAN measurements is 252.3 ± 0.73 deg and 8.7 ± 0.90 deg in ecliptic coordinates, which is off by about 3–4 deg from the He flow direction. The SWAN team speculates that this might be a sign of an asymmetry in the heliospheric interface due to the ambient interstellar magnetic field.

Comparing the above hydrogen temperature and velocity measurements by SWAN with heliospheric models leads to an estimate of the interstellar plasma density of $n_e \approx 0.04$ cm^{-3}. It is interesting to note that the plasma frequency for $n_e \approx 0.04$ cm^{-3} is 1.8 kHz, i.e. exactly the value of the remarkably stable cut-off frequency observed by Voyager.

Of particular interest for future studies might be the temperature minimum measured between the upwind and downwind directions. Classical models predict a monotonic increase in the line-of-sight temperature from upwind to downwind. The authors interpret this behaviour as first evidence of the existence of two distinct populations at different velocities, as predicted by some heliosphere/interstellar-gas interface models. If confirmed, this should provide a good diagnostic of the interface.

Total solar irradiance variations

The VIRGO instrument on SOHO extends the record of Total Solar Irradiance (TSI) measurements into cycle 23. In Figure 25, measurements from six independent space-based radiometers since 1978 (top) have been combined to produce the composite TSI over two decades (bottom). They show that the Sun's output fluctuates during each 11-year sunspot cycle, changing by about 0.1% between maxima (1980 and 1990) and minima (1987 and 1997) in solar activity. Temporary dips of up to 0.3% and a few days duration are the result of large sunspots passing over the

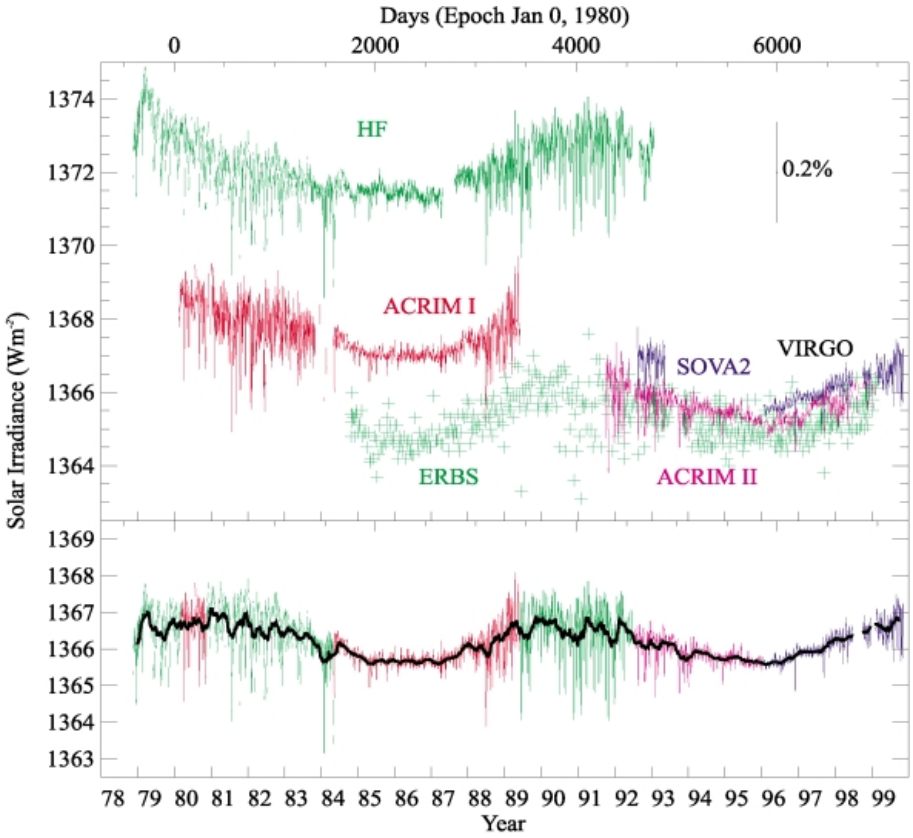

Figure 25. Total solar irradiance variations from 1978 to 1999. The data are from the Hickey-Frieden (HF) radiometer of the Earth Radiation Budget (ERB) experiment on Nimbus-7 (1978-1992), the two Active Cavity Radiometer Irradiance Monitors (ACRIM I and II) aboard the Solar Maximum Mission (1980-1989) and the Upper Atmosphere Research Satellite (1991-), respectively, and the VIRGO radiometers on SOHO (1996-). Also shown are the data from the radiometer on the ERB (1984-), and SOVA2 as part of the Solar Variability Experiment on the European Retrievable Carrier (1992-1993) (from Quinn and Fröhlich)

visible hemisphere. The larger number of sunspots near the peak in the 11-year cycle is accompanied by a general rise in magnetic activity that creates an increase in the luminous output which exceeds the cooling effects of sunspots. Offsets between the various data sets are the direct result of uncertainties in the absolute radiometer scale of the radiometers (±0.3%). Despite these biases, each data set clearly shows varying radiation levels that track the overall 11-year solar activity cycle.

Conclusions

SOHO set out to tackle three broad topics in solar and heliospheric physics: the structure and dynamics of the solar interior, the heating and dynamics of the solar corona, and the acceleration and composition of the solar wind. In all three areas, its observations have allowed great strides to be made in our understanding of the diverse physical processes at work in our Sun. This has been made possible by the comprehensive suite of state-of-the-art instruments mounted on the superb and stable SOHO spacecraft, operating from the unique vantage point of the L1 halo orbit.

In such complex areas of research as solar physics, progress is not made by just a few people acting in a vacuum. The scientific achievements of the SOHO mission are the results of a concerted, multi-disciplinary effort by a large international community of solar scientists, involving sound investments in space hardware, coupled with a vigorous and well-coordinated scientific operation and interpretation effort. The interplay between theory and observations has already provided many new insights and will continue to do so for many years.

With the wealth of SOHO data already in the archive (and many more data yet to come, hopefully well beyond the next solar maximum), we should be able to unravel even more of the mysteries of our closest star.

Acknowledgements

The great success of the SOHO mission is a tribute to the many people who designed and built this exquisite spacecraft and these excellent instruments, and to the many people who diligently work behind the scenes to keep it up and running. Special thanks go to: Harold W. Benefield and his AlliedSignal Flight Operations Team; Helmut Schweitzer and Jean-Philippe Olive from the ESA/MMS Technical Support Team; the Science Operations Co-ordinators Laura Roberts, Joan Hollis and Piet Martens; Craig Roberts, John Rowe and their colleagues from Flight Dynamics, the colleagues from DSN, and, last but not least, to Francis Vandenbussche and his recovery team for making a miracle come true!